METAL ORGANIC FRAMEWORKS FOR ENZYME IMMOBILIZATION IN BIOFUEL CELLS

by

JaDee Bodell

A thesis submitted to the faculty of
The University of Utah
in partial fulfillment of the requirements for the degree of

Master of Science

Department of Materials Science and Engineering

The University of Utah

December 2015

The University of Utah Graduate School

STATEMENT OF THESIS APPROVAL

The thesis of **JaDee Bodell**

has been approved by the following supervisory committee members:

Shelley D. Minteer	, Chair	**9/2/2015** Date Approved
Anil Vasudeo Virkar	, Member	**9/2/2015** Date Approved
Michael A. Scarpulla	, Member	**9/2/2015** Date Approved

and by **Feng Liu** , Chair/Dean of

the Department/College/School of **Materials Science and Engineering**

and by David B. Kieda, Dean of The Graduate School.

ABSTRACT

Interest in biofuel cells has been rapidly expanding as an ever-growing segment of the population gains access to electronic devices. The largest areas of growth for new populations using electronic devices are often in communities without electrical infrastructure. This lack of infrastructure in remote environments is one of the key driving factors behind the development of biofuel cells. Biofuel cells employ biological catalysts such as enzymes to catalyze oxidation and reduction reactions of select fuels to generate power. There are several benefits to using enzymes to catalyze reactions as compared to traditional fuel cells which use metal catalysts. First, enzymes are able to catalyze reactions at or near room temperature, whereas traditional metal catalysts are only efficient at very high temperatures. Second, biofuel cells can operate under mild pH conditions which is important for the eventual design of safe, commercially viable devices. Also, biofuel cells allow for implantable and flexible technologies. Finally, enzymes exhibit high selectivity and can be combined to fully oxidize or reduce the fuel which can generate several electrons from a single molecule of fuel, increasing the overall device efficiency.

One of the main challenges which persist in biofuel cells is the instability of enzymes over time which tend to denature after hours or days. For a viable commercial biofuel cell to be produced, the stability of enzymes must be extended to months or years. Enzymes have been shown to have improved stability after being immobilized. The focus of this research was to find a metal organic framework (MOF) structure which could

successfully immobilize enzymes while still allowing for electron transport to occur between the catalytic center of the enzyme and the electrode surface within a biofuel cell for power generation.

Four MOF structures were successfully synthesized and were subsequently tested to determine the MOF's ability to immobilize the following enzymes: nicotinamide adenine dinucleotide (NAD)-dependent alcohol and aldehyde dehydrogenases, and pyrroloquinoline quinone (PQQ)-dependent alcohol and aldehyde dehydrogenases, as well as flavin adenine dinucleotide (FAD)-dependent glucose dehydrogenase. Tb-meso MOF was shown to immobilize PQQ-dependent enzymes through π stacking interactions of the heme in the enzyme and the triazine molecules in the ligand of the MOF. However, the PQQ-dependent dehydrogenases did not have enough catalytic activity present to be measured electrochemically. Finally, ZIF-90 was synthesized under aqueous conditions in the presence of FAD-dependent glucose dehydrogenase (GDH) which led to size selective sheltering of FAD-GDH. FAD-GDH had activity an order of magnitude larger than any of the alcohol dehydrogenases, which provided sufficient catalytic activity to measure electrochemically. The FAD-GDH bound within ZIF-90 was used to build a full biofuel cell resulting in an open circuit voltage of 708 ± 16 mV and a maximum power density of 2.75 ± 0.40 $\mu W/cm^2$.

TABLE OF CONTENTS

LIST OF FIGURES

Figures

LIST OF ABBREVIATIONS

Ac-MWCNTs – anthracene modified multiwalled carbon nanotubes
ADH – alcohol dehydrogenase
ALDH – aldehyde dehydrogenase
BCA – bicinchoninic acid
BDC – 1,4-benzenedicarboxylic acid
BSA – bovine serum albumin
CV – cyclic voltammetry
DCM – dichloromethane
DCPIP – 2,6-dichlorophenol indophenol
DET – direct electron transfer
DHDBC – 2,5-dihydroxyl-1,4-benzenedicarboxylic acid
DHTP – 2,5-dihydroxyterephthalic acid
DMA – dimethylacetamide
DMF – N'N'-dimethylformamide
DMFc – dimethyl ferrocene
DMSO – dimethylsulfoxide
EGDGE – ethylene glycol diglycidyl ether
FAD – flavin adenine dinucleotide
GCE – glassy carbon electrode
GDH – glucose dehydrogenase
HEPES – 4-(2-hydroxyethyl)-1-piperazineethanesulfonic acid
LPEI – linear polyethylenimine
MET – mediated electron transfer
MOF – metal organic framework
NAD – nicotinamide adenine dinucleotide
NADP – nicotinamide adenine dinucleotide phosphate
NQSA – 1,2-naphthoquinone-4-sulfonic acid
PBSE – 1-pyrenebutanoic acid succinimidyl ester
PMS – phenazine methosulfate
PQQ - pyrroloquinoline quinone
TATB – 4,4'4,''-s-triazine-2,4,6-triyl-tribenzoic acid
TBAB- tetrabutylammonium bromide
ZIF – zeolitic imidazolate framework

CHAPTER 1

METAL ORGANIC FRAMEWORKS

1.1 Introduction

Metal organic frameworks (MOFs), also known as coordination polymers, were first synthesized in 1959 by Kinoshita et al.[1] However, the first coordination polymers synthesized during the 1950s and 1960s were unstable once solvent was removed and the structures would collapse, removing any porosity. Due to this instability, interest in coordination polymers largely faded and little research was focused on the subject until the 1990s when research groups such as those under the direction of Robson, Kitagawa, and Yaghi brought about renewed interest.[2,3] Yaghi et al. were the first group to coin the term MOF in a Nature article in 1999[4] with the introduction of MOF-5.

A metal organic framework is defined as a metallic cation or cluster of atoms which is then coordinated by organic linker molecules, referred to as ligands. The crystal coordination can occur in one, two, or three dimensions and results in a periodic structure which can be crystalline or amorphous. The specific geometry and structure of each MOF is determined by the preferred coordination of the metal ion or cluster along with the structure of the ligand. For example, Cu^{2+}, which has a preferred coordination number of 4, will generally exhibit either square pyramidal or tetragonal geometries,[5,6] whereas Co^{2+} has been shown to exhibit a coordination number of 6 and usually forms hexagonal structures.[7]

The synthesis of MOF-5 occurs through the coordination of Zn_4O clusters with 1,4-benzenedicarboxalate (BDC) ligands, resulting in a three-dimensional crystal structure of $Zn_4O(BDC)_3$ which is depicted in Figure 1.1. The dicarboxylate structure in ligands is now commonly used to achieve three-dimensional MOFs due to the bidentate coordination which provides for three-dimensional coordination. With the introduction of MOF-5, the first stable desolvated MOF to be reported, interest in the field was reinvigorated and the age of MOFs was born.

In the past fifteen years since the discovery of MOF-5, new MOF structures have been synthesized at a staggering pace. In comparison to zeolitic structures of which only 178 had been identified as of 2007[8], nearly 4000 MOF structures had already been synthesized.[9] With the ever-growing variety of MOF crystal structures available to researchers, MOFs have gained notoriety over the past decade as new structures have opened up their uses to a variety of applications including: gas storage, semiconductors, detergents, and catalysis to name a few. MOFs have been synthesized such that the cation is not fully coordinated by the ligands, leaving the metal clusters electrically or chemically active.

MOFs have been synthesized via a variety of techniques including: solvothermal, microwave, sonication, and electrochemical reactions.[10] Researchers have also functionalized the ligands in some structures, enabling complex chemical reactions to be facilitated. In order for the ligand to remain chemically active after chelation, the reactive group must be separate from the coordinating section of the ligand. Recently, interest in using MOFs as macroscopic scaffolds in which enzymes could be encapsulated within the structure for immobilization and in some cases, stabilization has been rapidly growing

for use in energy production, though the application in biofuel cells remains novel to the field.[11–13]

The focus of this thesis will be advancing the application of MOFs as frameworks in which to immobilize a series of enzymes for electrocatalysis in fuel cells. If MOFs can be used to create stable macroscopic frameworks in which to immobilize and stabilize enzymes, it may be possible to create viable enzymatic cascading catalysts which could then be used in biofuel cells for multiple oxidation reactions of complex fuels, generating multiple electrons from a single fuel molecule, as shown in Figure 1.2.

One advantage of MOFs to immobilize multiple enzymes onto an electrode in a fuel cell is ensuring that each enzyme in the cascade is in close proximity to one another. This minimizes diffusion lengths and increases the measurable power density and flux through the cascade pathway, and thus the overall efficiency of the fuel cell. A second advantage to immobilizing enzymes to MOFs prior to attaching to the electrode surface in a biofuel cell would be that the immobilization to the electrode would require only a single polymeric layer; previous research of enzymatic cascades has relied on multiple polymeric layers.[14] The multilayered structure inhibits diffusion of the fuel between the enzymes. This ultimately retards the transport of electrons to the electrode surface and thereby limits the efficiency of the fuel cell.

1.2 MOF Structures

1.2.1 Tb-meso MOF

The Tb-meso MOF forms a truncated octahedral structure which follows the Mobil Thirty-Nine (MTN) zeotype structure. Four Tb^{3+} moieties form a super tetrahedron (ST). Six of the ST are then coordinated with pairs of 4,4’,4’’-s-triazine-2,4,6-triyl-

tribenzoic acid (TATB) ligand molecules which pi stack about the triazine rings of the ligand and have the benzoate arms of the ligands off set such that each Tb^{3+} moiety in a ST is coordinated with six oxygen atoms from the deprotonated carboxylates. The crystal structure results in mesoporous cages of 3.9 nm and 4.7 nm in diameter which have 1.3 nm and 1.7 nm openings, respectively, as depicted in Figure 1.3. [15] The Tb^{3+} moieties are fully coordinated and as such, the metal sites are nonreactive, as can be demonstrated in some MOF structures, including the MOF-74 family.

The arrangement of the TATB ligands are of particular interest due to the stacking of the triazine rings. The coordinated π-π stacking exhibited in Tb-meso MOF creates an extended orbital which can exert a much larger interaction force than a single ligand and plays a key role in enzyme immobilization. Enzymes which contain a heme structure have been reported[16] to be immobilized through π-π stacking interactions, as will be discussed in further detail in Chapter 2. This is the first known reported MOF which has exhibited enzyme immobilization simply through ligand-enzyme interactions.

1.2.2 Zn MOF-74

Zn MOF-74 is comprised of zinc cations coordinated with five oxygen atoms from three 2,5-dihydroxyterephthalic acid (DHTP) ligands. The asymmetric bonding of DHTP to the zinc ions results in an asymmetric paddlewheel structure that when the structure is extended, the resulting pores have a hexagonal rod-like structure, as is depicted in Figure 1.4. The MOF-74 family structures retain a cubic topology, as in MOF-5, the parent MOF which also contained Zn_4O clusters as the metallic nodes. Zn^{2+} has a coordination of six. The resulting crystal structure therefore is under-coordinated. As a result of the under-coordination, the zinc ions are both chemically and electrically

active. The hexagonal pores have a diameter of 1.4 nm with a length dependent on grain size. Similar extended MOF-74 structures with pore sizes as large as 8.5 nm have been created using a terephthalate base structure with up to nine phenyl groups attached between the carboxylic acid ends of the terephthalate which were utilized for the ligands, as has been previously reported.[17]

1.2.3 Cu BPTC MOF

The Cu biphenyl-3,3',5,5'-tetracarboxylic acid (BPTC) MOF is centered on a pair of Cu^{2+} ions which have a coordination number of 5, resulting in a square pyramidal geometry. Each Cu^{2+} ion is coordinated with four carboxylate groups, resulting in distorted paddlewheels which are interconnected due to the asymmetry of the ligand, as can be seen in Figure 1.5. The crystal structure exhibits an NbO topology which has approximately 0.7 nm pores in a perfect crystal.[18]

One of the enzyme immobilization techniques which will be detailed in Chapter 2 relies on molecules which include a pyrene subunit being able to π-π stack. This pi stacking has been experimentally observed in pyrene on carbon nanotubes, as has been previously reported.[19] The mechanism of π stacking will be discussed in further detail in Chapter 2. The Cu BPTC MOF structure was tested to see if enough planar characteristic was present between either the ligands along the c axis, or the copper clusters visible from the a axis and the pyrene to enable enzyme immobilization.

1.2.4 ZIF-90 MOF

Zeolitic Imidazolate Framework (ZIF) MOF structures, as implied by their naming conventions, have similar structures to that of inorganic zeolites and exhibit a

sodalite (SOD) topology, as depicted in Figure 1.6.[20,21] The Zn^{2+} ions are coordinated with four nitrogen atoms as well as two oxygen atoms from the 2-imidazolecarboxaldehyde (ICA) ligands fully coordinating the Zn^{2+} ions. The largest pore diameter is 0.35 nm with a pore window of 0.11 nm.[22] While the porosity of ZIF-90 is at least an order of magnitude too small for enzymes, particularly large enzymes such as dehydrogenases, to enter into the pores, the synthesis steps offer a different approach to enzyme immobilization.

ZIF-90 can be synthesized at room temperature under aqueous conditions, which allows the enzymes to be present during assembly, which allows for size selective sheltering of the enzymes. This form of entrapment is a physical immobilization as opposed to a chemical interaction. The benefits and risks of this technique will be explained in more detail and compared to traditional immobilization techniques in Chapter 2.

1.2.5 MMCF-2 MOF

The metal-macrocyclic framework-2 (MMFC-2) MOF has a large planar ligand with a tetraazacyclododecane center which resembles the nitrogen-based center of a heme structure, both of which can be seen in Figure 1.7. MMCF-2 exhibits an extended NbO topology wherein the Cu^{2+} ions are coordinated in a square planar fashion with one oxygen atom from four separate ligands. The resulting paddlewheel structure forms the secondary building units of the crystal structure which join together which form as a cuboctahedral structure, as depicted in Figure 1.7.[23]

While MMCF-2 does not incorporate the full polyporphyrin molecule as present in a heme, the hypothesis was that the four nitrogen atoms present in the 1,4,7,10-

tetraazocyclododecane molecule, also known by the trade name Cyclen, would present an adequate π orbital for enzyme immobilization. This could be accomplished either through direct π- π interaction of the ligand and a heme if present in the enzyme, or through the immobilization of a pyrene-based molecule, as will be discussed in detail later.

1.3 Experimental

All chemicals and reagents used for MOF synthesis were purchased from Sigma-Aldrich and used as purchased unless specifically stated otherwise within the individual procedures below.

1.3.1 Tb-meso MOF

1.3.1.1 TATB Synthesis

This molecule was prepared according to a previously reported procedure.[15] In a 50 mL round bottom flask, 2.9 mL of p-tolunitrile was slowly added to 10 g trifluoromethanesulfonic acid and stirred under atmospheric conditions for 13 hours. The mixture was then poured on ice and the pH neutralized with concentrated ammonium hydroxide. The precipitate was then filtered out and thoroughly rinsed with water followed by acetone. Recrystallization of the crude material in toluene provides the intermediate product 2,4,6-tri-p-tolyl-s triazine [1] which is depicted in Figure 1.8.

Next, 2.78 g of [1], 70 mL acetic acid, and 4.4 mL concentrated H_2SO_4 were added to a 500 mL three-necked flask which was placed in a water bath and the solution was stirred vigorously. 7.2 g CrO_3 along with 4.8 mL of acetic anhydride were then added to the solution over the course of 10 minutes, ensuring that the temperature did not exceed 50 C, and allowed to stir overnight. The slurry was then added to 300 mL DI

water, and stirred for 10 minutes prior to filtering the solid residue. The solid was then dissolved into 200 mL 2 N sodium hydroxide and filtered to remove any unreacted material. The filtered solution was re-acidified with concentrated HCl to precipitate out the crude product. Recrystallization in DMF produced pure 4,4',4''-s-triazine-2,4,6-triyl-tribenzoic acid (TATB) as a white solid. The H^1NMR spectra and chemical structure of TATB can be seen in Figure 1.9.[24] The peaks at 8.7 and 8.1 MHz represent the hydrogens on the benzene rings closest to the carboxylate, and triazine rings, respectively. All other peaks either represent solvents used during synthesis or were unable to be identified but are unrelated to TATB.

1.3.1.2 Tb-meso MOF Synthesis

Synthesis was performed as previously reported with a minor modification to the temperature of solvothermal synthesis as no crystals were formed following the temperature in the previously reported procedure.[15] In summary, 30 mg of terbium nitrate hydrate and 10 mg of TATB were added to a 20 mL vial with 2 mL DMA, 0.4 mL methanol and 0.1 mL DI water. The vial was capped and placed in an oven for 2 days which was preheated to 125 C, resulting in autogenous pressure inside the vial. After holding at temperature, the sample was then cooled at a rate of 10 C/hr to ambient in order to form colorless crystals. The crystals were then filtered to remove solvent and dried under vacuum at 105 C to remove guest molecules.[15] The FTIR spectrum of Tb-meso MOF can be seen in Figure 1.10. The peaks at 1648 cm^{-1} was attributed to the COO^- bond of the guest molecule DMA. The peaks at 1535 cm^{-1} and 1377 cm^{-1} have been assigned the assymetric bonds of the COO^- in the TATB ligand.[15]

1.3.2 Zn MOF-74 Synthesis

Synthesis of Zn MOF-74 was completed through the combination of two previous literature protocols. The first demonstrated the possibility of room temperature synthesis of several MOFs including MOF-74.[25] The second described how allowing the MOF framework to remain in an over-solvated state for extended periods would result in the creation of semi-amorphous regions, resulting in a mesoporous structure. The formation of a semi-amorphous structure allowed pores as large as 20 nm to be formed by forming large voids which were encased by the smaller porous crystalline structure.[26]

240 mg of DHTP, the structure of which can be seen in Figure 1.11, and 686 mg of zinc acetate dihydrate ($Zn(OAc)\cdot 2H_2O$) were each independently dissolved in 20 mL of DMF. The two solutions were then mixed and stirred vigorously. The amount of time the solutions were stirred was varied and will be denoted henceforth as Zn MOF-74/t, where t is the time in hours allowed to stir in DMF. The resulting crystals were separated from the solvent via filtration and dried under vacuum at 105 C to remove guest molecules remaining from synthesis. The simplicity of synthesis is likely one of the contributing reasons the structure has been so extensively studied.[26–28]

1.3.3 Cu BPTC Synthesis

Synthesis of the Cu BPTC MOF was completed according to a previously reported procedure.[18] A 15 mL solution of DMF/1,4-dioxane/H_2O (1:1:2 v/v/v) was freshly prepared in a 20 mL glass vial. To the solution, 0.04 g BPTC and 0.10 g $Cu(NO_3)_2\cdot 2.5H_2O$ were added along with the addition of two drops of concentrated aqueous HCl. The solution was then capped and placed in an oven which was ramped from ambient temperature up to 80 C at a rate of 5 C/hr. The solution was held at temperature

for 3 days. The solution was then cooled to 50 C at a rate of 5 C/hr at which point the blue crystals were filtered and thoroughly washed with a mixture of DMF and H_2O (1:2 v/v) followed by rinsing with pure DMF. The blue crystals were then dried under vacuum at ambient temperature.[18]

1.3.4 ZIF-90 Synthesis

Synthesis of ZIF-90 was accomplished at room temperature in aqueous conditions and, as such, is the most environmentally friendly synthesis considered in this thesis. Procedures were completed as previously described. In brief, 371 mg of $Zn(NO_3)\cdot 6H_2O$ was dissolved in 18 MΩ-cm ultrapure water. Next, 480 mg of ICA and 50 mg (40,000 MW) PVP were separately dissolved in 25 mL 18 MΩ-cm water at 42 C under vigorous stirring. The zinc nitrate solution was added to the ligand/polymer solution and stirred for 10 minutes. ZIF-90 formed as a white precipitate in water which was collected by centrifugation (5,000 g for 15 min). The solid was then thoroughly washed with ultrapure water at least 5 times and was then dried under vacuum.[29]

1.3.5 MMCF-2

1.3.5.1 H_4tactmb Synthesis

H_4tactmb was first synthesized according to a previously reported method.[23] 516 mg of Cyclen and 3.3 g methyl 4-(bromomethyl)benzoate were dissolved in 200 mL acetonitrile. 4.0 g of potassium carbonate was then slowly added over 10 minutes. The mixture was then refluxed while stirring vigorously for 24 hours. The solvent was then removed through evaporation under vacuum and the solid residue was then dissolved in dichloromethane (DCM) and partitioned with water. The water phase was then separated

from the organic phase with three separate washes of 100 mL of DCM. The organic mixture was then evaporated down to 100 mL to remove excess solvent and was then washed with 6 M sodium chloride brine solution prior to drying with sodium sulfate. After drying, the organic mixture had excess solvent removed through evaporation down to a small volume, at which point the intermediate product (1.21 g, 54.5%) was crystallized from a mixture of hexane and ethyl acetate (10:1 v/v).

This solid was then dissolved in 100 mL methanol, to which 5 mL of 3.4 mM potassium hydroxide was added and the solution was refluxed for 18 hours. The methanol was evaporated under vacuum and the solution was neutralized using 1 M HCl and then rinsed with water. The final product (0.81 g, 55%) was filtered and then freeze dried for preservation. The resulting H NMR spectrum is displayed in Figure 1.12. The peaks at 7.9 and 7.4 MHz have been assigned to the hydrogen on the benzene rings closest to the Cyclen and carboxylates, respectively. Lastly, the peak at 3.9 MHz are the 16 hydrogens present within the Cyclen molecule.[23]

1.3.5.2 MMCF-2 Synthesis

Synthesis of MMCF-2 was attempted as previously reported but no crystal formation was attained. In a 20 mL glass vial, 1 mg of H_4tactmb and 3 mg of $Cu(NO_3)\cdot 2.5H_2O$ were dissolved in 1 mL DMA. Two drops of 47% aqueous HBF_4 were added which is reported to be necessary for crystal formation. The procedure states that the sample should be heated at 85 C for 3 days. No ramp rates were noted in the paper. Both 5 and 10 C/hr were attempted as well as attempting higher temperatures of 95 and 105 C but none of these attempts resulted in crystal formation.[30]

1.4 Conclusions

This chapter has introduced the concept of metal organic frameworks and the description of five different MOF structures were described in detail. Four MOF structures were successfully synthesized. Each MOF structure has unique properties which were tested as scaffolds for enzyme immobilization in the use of biofuel cells, as will be discussed in Chapter 2. Herein is a review of the MOFs which were synthesized and characterized for biofuel cell applications.

First, Tb-meso MOF has been previously reported to immobilize MP-11 through π-π stacking between the heme structure in the enzyme and the triazine rings in the TATB ligand.[16] Other enzymes which contain a heme are then good candidates for enzyme immobilization with Tb-meso MOF. Zn MOF-74 was the second structure synthesized and was of interest for two reasons. The first reason was the ability to control the pore size of the structure by introducing amorphous character through extended periods of solvation. Secondly, the active zinc sites provide the possibility of chemical interaction leading to immobilization. Cu BPTC MOF and, had it been able to be produced, MMCF-2 were both synthesized to test planar MOF structures and their ability to either directly immobilize enzymes, as has been shown with Tb-meso MOF, or through the addition of a pyrene-based linker molecule to facilitate immobilization.

Finally, ZIF-90 was chosen as a means of physical entrapment of enzymes, rather than chemical bonding or surface interactions. Aqueous synthesis allow for the incorporation of enzymes during synthesis of the MOF, resulting in size-selective sheltering. This form of entrapment is not suitable for all enzymes, which will be discussed further in Chapter 2.

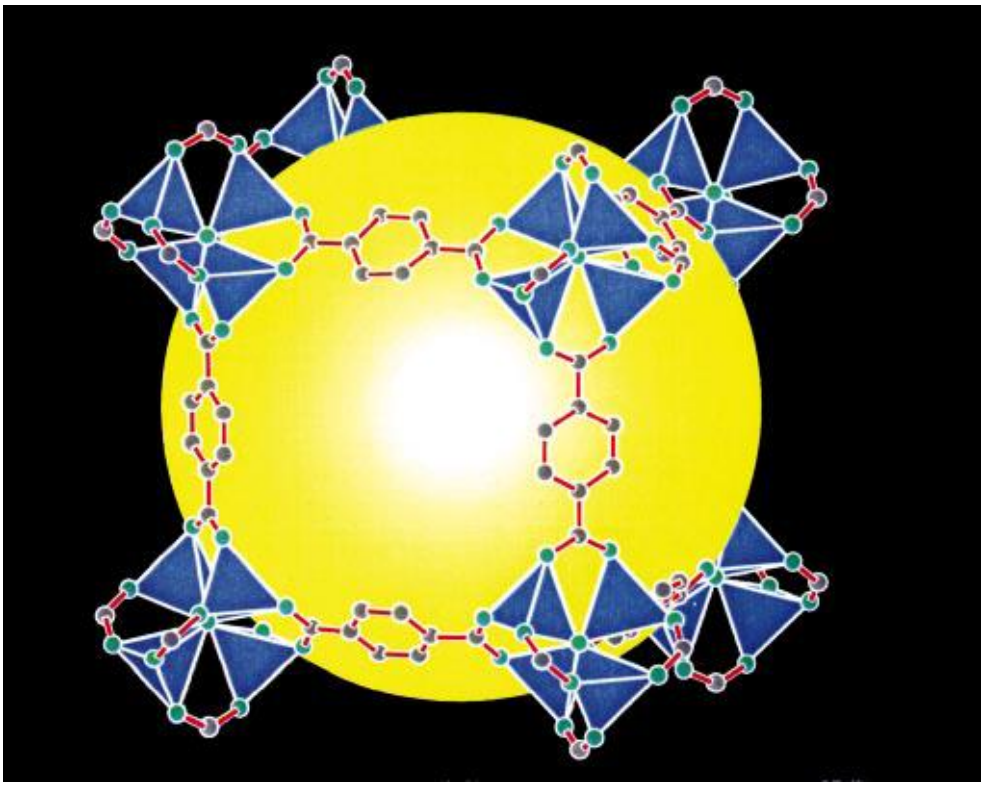

Figure 1.1: MOF-5 structure displaying the 18.5 Å diameter pore as the yellow sphere. O, green; C, grey; ZnO_4 tetrahedra shown in blue. Reprinted with permission from [4]. Copyright (1999) Nature

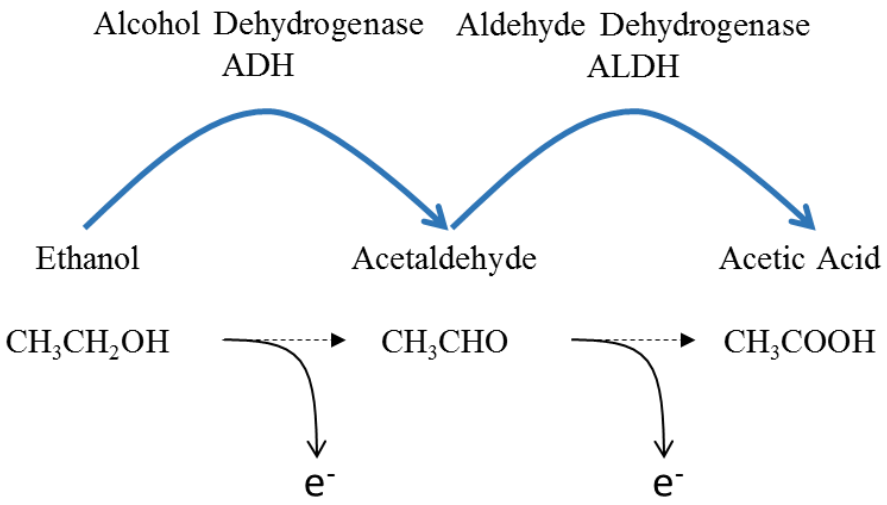

Figure 1.2: Oxidation pathway of ethanol to acetic acid via ADH and ALDH.

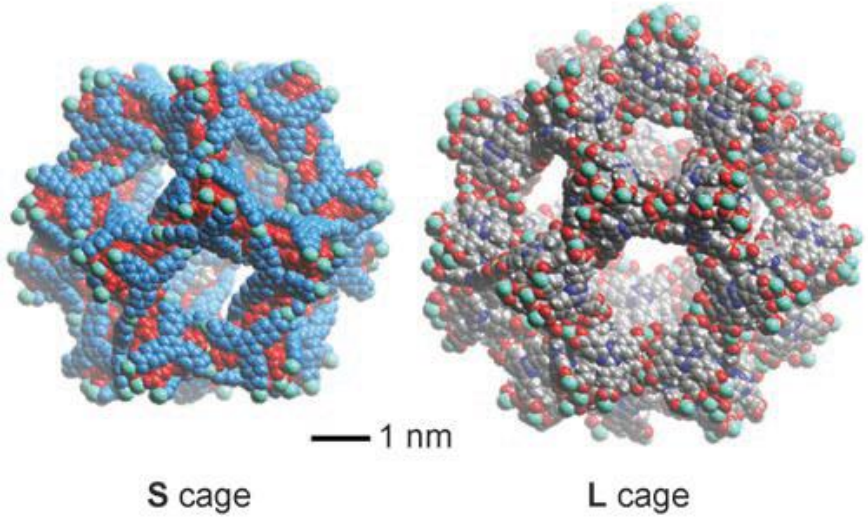

Figure 1.3: The S (small) and L (large) cages of Tb-meso MOF drawn as space-filling models. In the S cage, the inner TATB ligands are drawn in red, and outer ligand in blue; in the L cage, (C, grey; H, white; N, blue; O, red; Tb, light blue). Reprinted with permission from [15]. Copyright (2007) Angewandte Chemie International Edition.

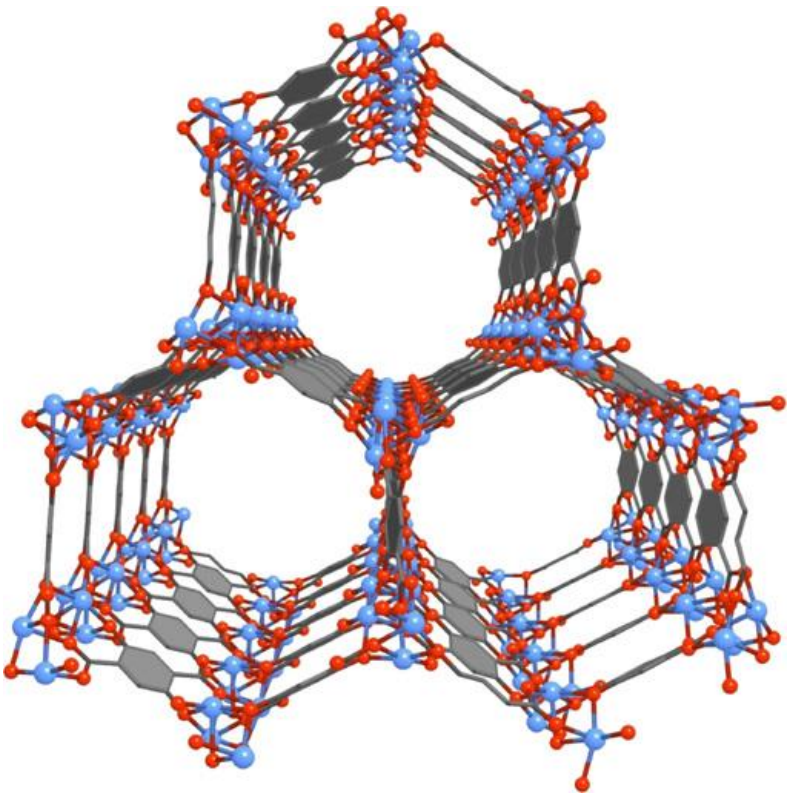

Figure 1.4: Zn MOF-74 structure: zinc blue, oxygen red, carbon grey
Reprinted with permission from [17]. Copyright (2011) Chemical Engineering Science.

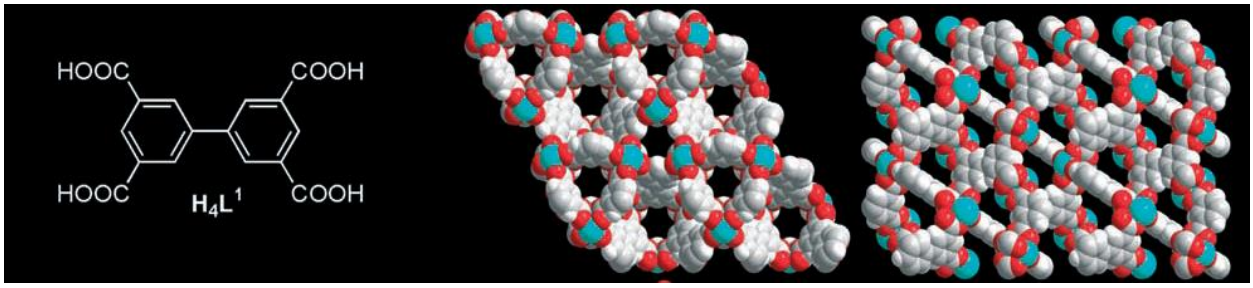

Figure 1.5: Cu-BPTC MOF structure. Left: Chemical structure of BPTC, Center: Cu BPTC as viewed from c axis, Right: Cu BPTC viewed from the a axis. Copper, blue; oxygen, red; carbon, white. Reprinted with permission from [18]. Copyright (2006) Angewandte Chemie International Edition.

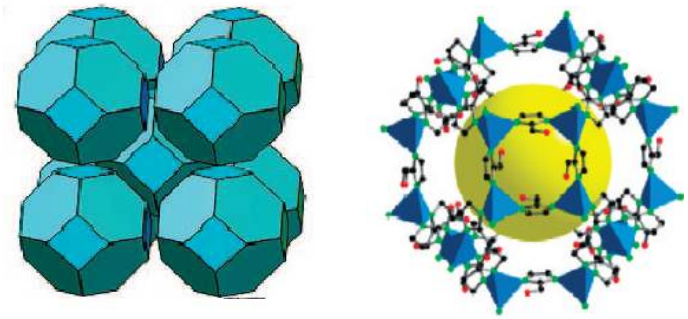

Figure 1.6: ZIF-90 topology and structure. Left: SOD topology exhibited by ZIF-90. Reprinted with permission from [20]. Copyright (2012) RSC Advances.Right: ZIF-90 ball and stick structure (ZnN_4 tetrahedra, blue; O, red; N, green; C, black; the pore volume is represented by the yellow sphere). Reprinted with permission from [21]. Copyright (2010) ACS.

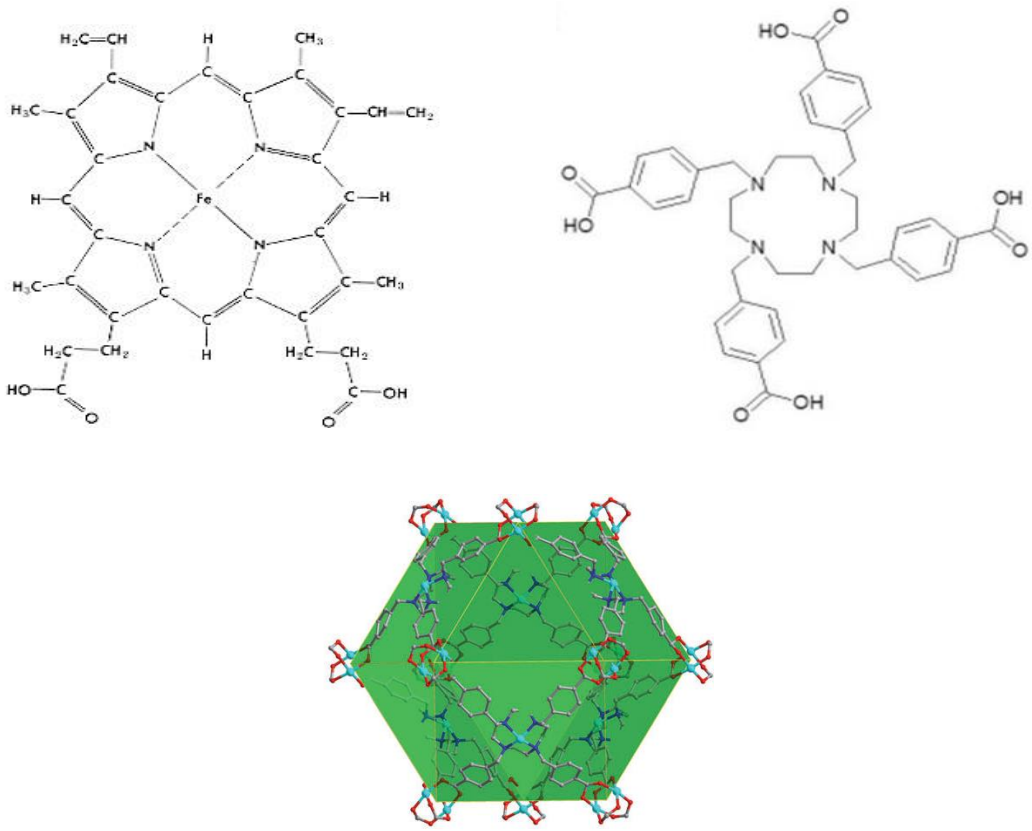

Figure 1.7: MMCF-2 and heme comparison. Left: Heme chemical structure. Right: H_4tactmb ligand chemical structure. Bottom: MMCF-2 crystal structure (O, red; N, dark blue; C, grey; Cu, light glue). Reprinted with permission from [22]. Copyright (2014) Angewandte Chemie International Edition.

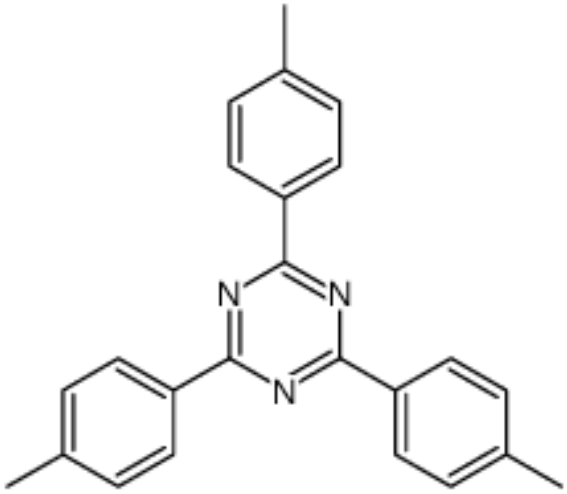

Figure 1.8: Chemical structure of 2,4,6-tri-p-tolyl-s triazine [1]

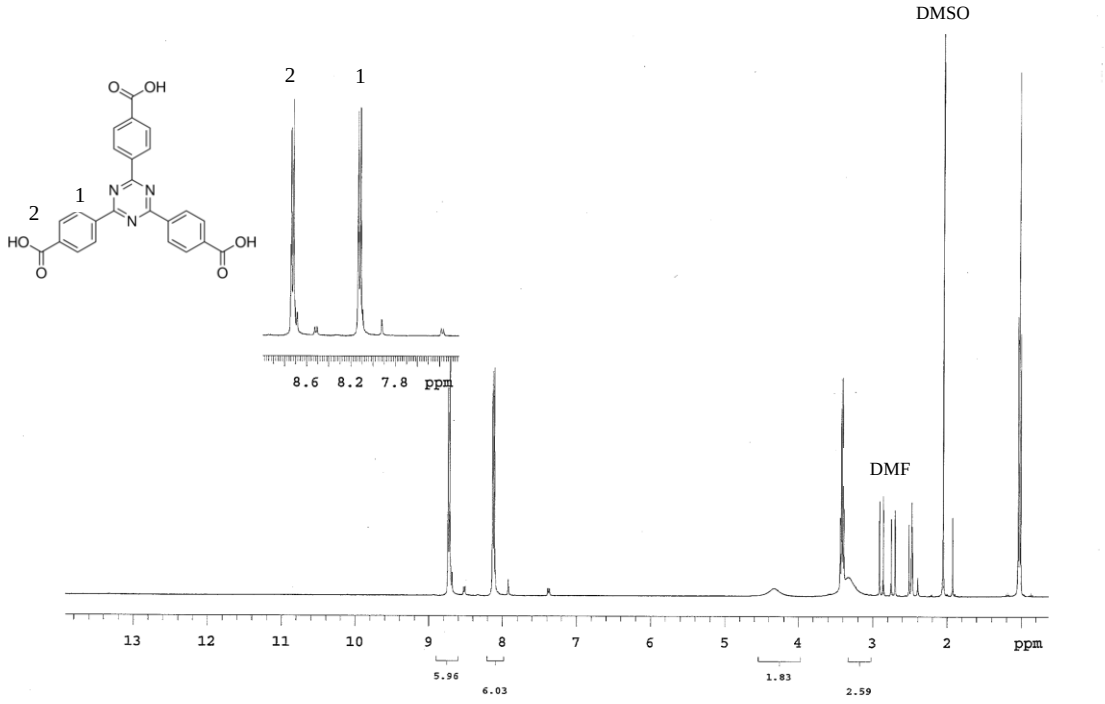

Figure 1.9: H^1 NMR (300 MHz, DMSO-d_6) spectra of TATB with chemical structure depicted: δ 8.7 MHz (d, 6 H) 8.1 MHz (d, 6 H).

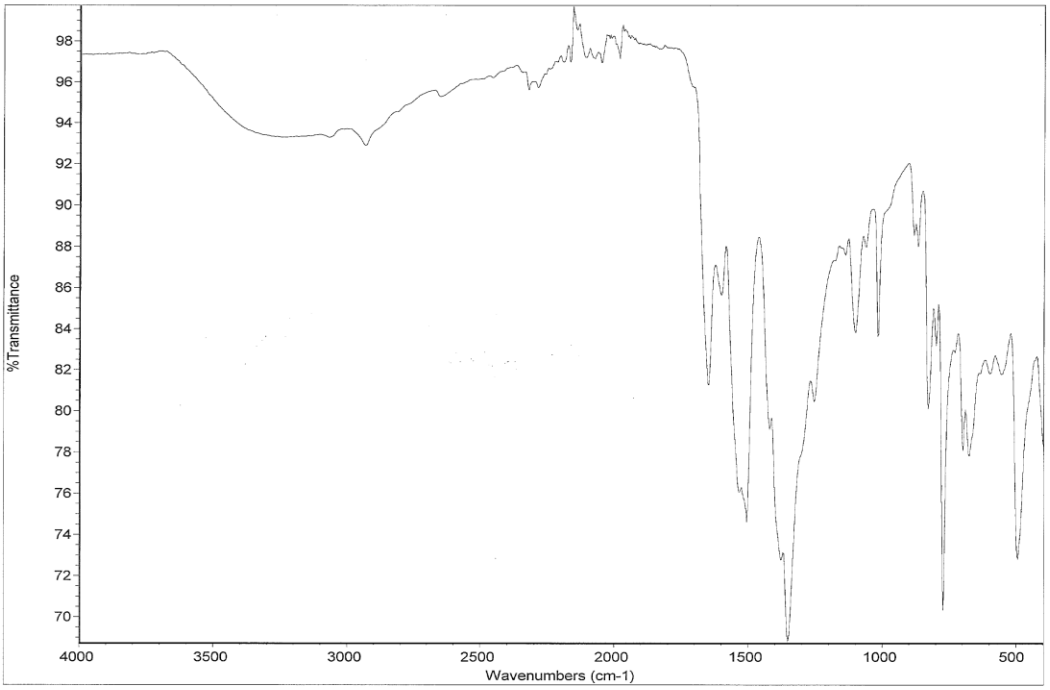

Figure 1.10: FTIR spectra of Tb-meso MOF peaks located at: 3380 cm^{-1} (w. br), 2930 cm^{-1} (w), 1648 cm^{-1} (s), 1535 cm^{-1} (s), 1504 cm^{-1} (s), 1377 cm^{-1} (s), 1349 cm^{-1} (s), 1252 cm^{-1} (m), 1061 cm^{-1} (m), 1016 cm^{-1} (vs), 882 cm^{-1} (s), 867 cm^{-1} (vs), 828 cm^{-1} (s), 773 cm^{-1} (vs), 700 cm^{-1} (m), 670 cm^{-1} (w), 602 cm^{-1} (s), 551 cm^{-1} (m), 495 cm^{-1} (s), 451 cm^{-1} (m).

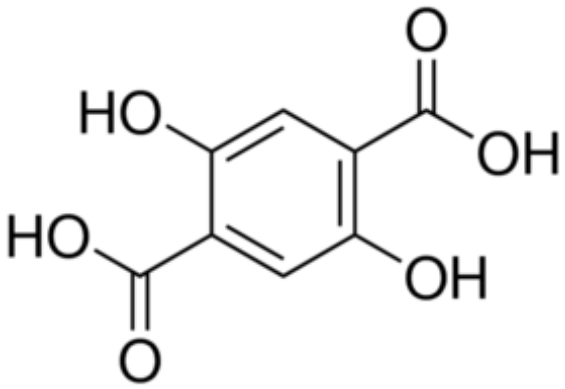

Figure 1.11: Chemical structure of DHTP

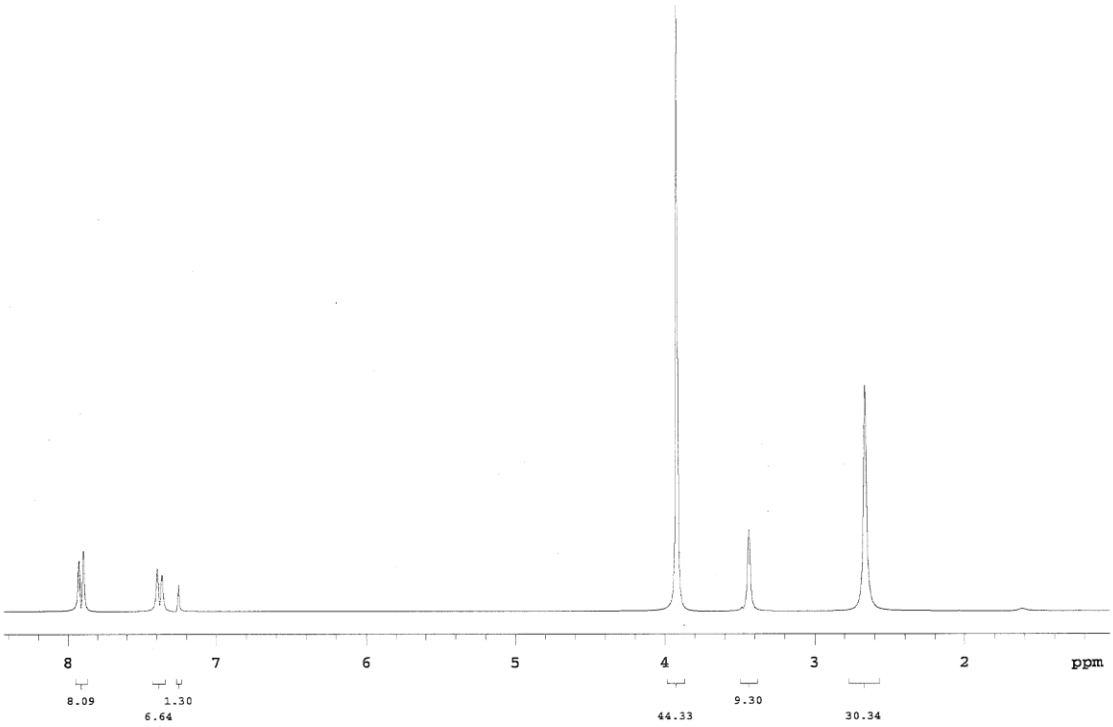

Figure 1.12: H NMR spectra of H_4tactmb: δ 7.9 MHz (d, 8 H), 7.4 MHz (d, 8 H), 3.95 MHz (d, 16 H). Other peaks attributed to remaining solvents from synthesis.

1.5 References

(1) Kinoshita, Y.; Matsubara, I.; Saito, Y. *Bull. Chem. Soc. Jpn.* **1959**, *32* (11), 1216–1221.

(2) Juan-Alcaniz, J. Engineering of Metal Organic Framework Catalysts, TU Delft, Delft University of Technology, 2013.

(3) Corma, A.; García, H.; Llabrés i Xamena, F. X. *Chem. Rev.* **2010**, *110* (8), 4606–4655.

(4) Li, H.; Eddaoudi, M.; O'Keeffe, M.; Yaghi, O. M. *Nature* **1999**, *402* (6759), 276–279.

(5) Carson, C. G.; Hardcastle, K.; Schwartz, J.; Liu, X.; Hoffmann, C.; Gerhardt, R. A.; Tannenbaum, R. *Eur. J. Inorg. Chem.* **2009**, *2009* (16), 2338–2343.

(6) Lincke, J.; Lässig, D.; Moellmer, J.; Reichenbach, C.; Puls, A.; Moeller, A.; Gläser, R.; Kalies, G.; Staudt, R.; Krautscheid, H. *Microporous Mesoporous Mater.* **2011**, *142* (1), 62–69.

(7) Livage, C.; Guillou, N.; Castiglione, A.; Marrot, J.; Frigoli, M.; Millange, F. *Microporous Mesoporous Mater.* **2012**, *157*, 37–41.

(8) Baerlocher, C.; McCusker, L. B.; Olson, D.; Meier, W. M.; International Zeolite Association; Structure Commission. *Atlas of zeolite framework types*; Published on behalf of the Structure Commission of the International Zeolite Association by Elsevier: Amsterdam; Boston, 2007.

(9) Long, J. R.; Yaghi, O. M. *Chem. Soc. Rev.* **2009**, *38* (5), 1213.

(10) Stock, N.; Biswas, S. *Chem. Rev.* **2012**, *112* (2), 933–969.

(11) Gu, Q. Self assembly for surface functionalization to improve biocompatibilities in Ti-based implants and enzyme immobilization in biofuel cells, Faculty of Engineering of the University of London School of Engineering and Materials Science Queen Mary, University of London, 2010.

(12) Safdar, M.; Sproß, J.; Jänis, J. *J. Chromatogr. A* **2014**, *1324*, 1–10.

(13) Feng, D.; Liu, T.-F.; Su, J.; Bosch, M.; Wei, Z.; Wan, W.; Yuan, D.; Chen, Y.-P.; Wang, X.; Wang, K.; Lian, X.; Gu, Z.-Y.; Park, J.; Zou, X.; Zhou, H.-C. *Nat. Commun.*

2015, *6*, 5979.

(14) Sokic-Lazic, D.; Minteer, S. D. *Biosens. Bioelectron.* **2008**, *24* (4), 939–944.

(15) Park, Y. K.; Choi, S. B.; Kim, H.; Kim, K.; Won, B.-H.; Choi, K.; Choi, J.-S.; Ahn, W.-S.; Won, N.; Kim, S.; Jung, D. H.; Choi, S.-H.; Kim, G.-H.; Cha, S.-S.; Jhon, Y. H.; Yang, J. K.; Kim, J. *Angew. Chem.* **2007**, *119* (43), 8378–8381.

(16) Chen, Y.; Han, S.; Li, X.; Zhang, Z.; Ma, S. *Inorg. Chem.* **2014**, *53* (19), 10006–10008.

(17) Deng, H.; Grunder, S.; Cordova, K.; Valente, C.; Yaghi, O. M. *Science* **2012**, *336* (6084), 1018–1023.

(18) Lin, X.; Jia, J.; Zhao, X.; Thomas, K. M.; Blake, A. J.; Walker, G. S.; Champness, N. R.; Hubberstey, P.; Schröder, M. *Angew. Chem. Int. Ed.* **2006**, *45* (44), 7358–7364.

(19) Chen, R. J.; Zhang, Y.; Wang, D.; Dai, H. *J. Am. Chem. Soc.* **2001**, *123* (16), 3838–3839.

(20) Amrouche, H.; Creton, B.; Siperstein, F.; Nieto-Draghi, C. *RSC Adv.* **2012**, *2* (14), 6028.

(21) Phan, A.; Doonan, C. J.; Uribe-Romo, F. J.; Knobler, C. B.; O'Keeffe, M.; Yaghi, O. M. *Acc. Chem. Res.* **2010**, *43* (1), 58–67.

(22) MOFomics - Pore Characterization of ZIF-90 (sod) http://helios.princeton.edu/mofomics/cgi-bin/view_structure.pl?src=user&id=1729b7f4d34e27c2d4f6cad8132eadde (accessed May 22, 2015).

(23) Gao, W.-Y.; Niu, Y.; Chen, Y.; Wojtas, L.; Cai, J.; Chen, Y.-S.; Ma, S. *CrystEngComm* **2012**, *14* (19), 6115.

(24) Sun, D.; Ma, S.; Ke, Y.; Collins, D. J.; Zhou, H.-C. *J. Am. Chem. Soc.* **2006**, *128* (12), 3896–3897.

(25) Tranchemontagne, D. J.; Hunt, J. R.; Yaghi, O. M. *Tetrahedron* **2008**, *64* (36), 8553–8557.

(26) Yue, Y.; Qiao, Z.-A.; Fulvio, P. F.; Binder, A. J.; Tian, C.; Chen, J.; Nelson, K. M.; Zhu, X.; Dai, S. *J. Am. Chem. Soc.* **2013**, *135* (26), 9572–9575.

(27) Grant Glover, T.; Peterson, G. W.; Schindler, B. J.; Britt, D.; Yaghi, O. *Chem. Eng. Sci.* **2011**, *66* (2), 163–170.

(28) Peterson, G. W.; Mahle, J.; Balboa, A.; Wagner, G.; Sewell, T.; Karwacki, C. J. *Evaluation of MOF-74, MOF-177, and ZIF-8 for the Removal of Toxic Industrial Chemicals*; DTIC Document, 2008.

(29) Shieh, F.-K.; Wang, S.-C.; Yen, C.-I.; Wu, C.-C.; Dutta, S.; Chou, L.-Y.; Morabito, J. V.; Hu, P.; Hsu, M.-H.; Wu, K. C.-W.; Tsung, C.-K. *J. Am. Chem. Soc.* **2015**, *137* (13), 4276–4279.

(30) Gao, W.-Y.; Chen, Y.; Niu, Y.; Williams, K.; Cash, L.; Perez, P. J.; Wojtas, L.; Cai, J.; Chen, Y.-S.; Ma, S. *Angew. Chem. Int. Ed.* **2014**, *53* (10), 2615–2619.

CHAPTER 2

ENZYMES AND IMMOBILIZATION

2.1 Introduction

2.1.1 Enzyme Overview

Enzymes are a class of proteins which function as biological catalysts. Enzymes can range in size from a few thousand Daltons, to well into the hundreds of thousands of Daltons. Many enzymes are comprised of smaller subunits which complex together and in some cases, catalytic activity can be observed from a single monomer, as in DNA polymerase I of *Escherichia coli*.[1] However, there are examples of oligomeric enzymes which exhibit no catalytic activity when the individual monomers are not fully complexed, such as in the case of reverse transcriptase which relies on the complexing of polymerase with nuclease in order to create DNA from RNA.[2]

Whereas monomeric enzymes rely on the tertiary structure of an enzyme folding about itself to facilitate catalytic activity, oligomeric enzymes often rely on the quaternary structure of the individual monomers joining together to provide the necessary geometry to enable catalysis. The degree of complexity and orientation of the subunits present in a specific enzyme will determine the degree of specificity to which substrates are susceptible to catalysis. Some enzymes exhibit broad specificity for catalysis such as pepsin which is found in the human digestive tract. As such, having a broad specificity to catalyze most proteins into smaller peptides is key to digestion. Most enzymes, however,

exhibit a narrow specificity, such as alcohol dehydrogenases which are only able to oxidize a few select alcohols to aldehydes, such as methanol and ethanol but not larger alcohols.[3]

The following sections describe the enzymes employed in this research, alcohol dehydrogenases (ADH) and aldehyde dehydrogenases (ALDH) purified from two species, *Saccharomyces cerevisiae* and *Gluconobacter* as well as glucose dehydrogenase (GDH) purified from *Aspergillus sp*. The dehydrogenase class of enzymes which catalyze the oxidation of a desired substrate by enabling hydride transfer from the fuel, and in turn reduces a cofactor. For the enzymes covered in this thesis, three separate cofactors are used by the different enzymes. For those enzymes purified from *S. cerevisiae*, NAD^+ or $NADP^+$ are used as the cofactors, which are then reduced to NADH or NADPH, respectively, upon the oxidation of the fuel. Electrochemical regeneration of NAD^+ or $NADP^+$ is then needed for the use of these enzymes in biosensors or biofuel cells.

In contrast, the enzymes which have been purified from *Gluconobacter*, are PQQ-dependent for oxidation of substrate to occur, in which PQQ is reduced by the hydride and then the heme centers of the enzymes act as electron acceptors to complete the reaction and communicate with an electrode. PQQ is part of the quaternary structure of the enzyme and, as such, it is not readily depleted, as in the case of the NAD-dependent enzymes which is consumed and must either be replenished or the NADH oxidized from an external source, such as an electrode. The GDH purified from *Aspergillus sp.* is dependent on flavin adenine dinucleotide (FAD), which like PQQ is bound within the quaternary structure of the enzyme. Finally, laccase which was purified from *Trametes versicolor* was utilized for the reduction of oxygen to water. Laccase can catalyze oxygen

reduction without the use of mediator, but in the presence of electron acceptors, laccase is also able to facilitate the reduction of several nonphenolic compounds besides oxygen due to the nonselective metallic active site.

2.1.1.1 NAD-ADH

There have been 7 different NAD-ADH enzymes isolated from baker's yeast (*Saccharomyces cerevisiae*) and while each enzyme exhibits unique variations, the fundamental catalytic structure is similar to that of ADH1 which is described here in detail. ADH1 has a molecular weight of 150 kDa consisting of four identical monomers which join to form the quaternary structure. The approximate calculation of the diameter of the enzyme if it is assumed to be spherical is shown in Eq. 2.1.[4] Using Eq. 1, ADH1 can be approximated to have a diameter of 15 nm. This is an overestimation by approximately fifty percent due to the asymmetry present in ADH1, as the enzyme has been experimentally observed by Malvern Instruments© to have a diameter of 9.8 nm along its greatest axis.[5] While the simplified equation does not perfectly fit experimental results, the calculation provides a rough estimation for initial inquiries.

$$D\ (nm) = 0.284 * \sqrt[3]{M}\ (Da) \qquad \text{(Eq. 2.1)}$$

The active catalyst site is a zinc ion which binds the alcohol and facilitates the hydride transfer to the cofactor. For ADH1, there is one active zinc site per monomer, resulting in four active centers per enzyme. A second zinc site participates in enzyme folding and maintains the quaternary structure. Either NAD^+ or $NADP^+$ can be used as a cofactor, the structures of which can be found in Figure 2.1. The cofactor is required for catalysis such that the cofactor is reduced upon alcohol oxidation to the corresponding aldehyde to maintain electroneutrality. NAD-ADH shows the highest affinity for

oxidizing ethanol, but has also been reported to oxidize methanol.[6]

2.1.1.2 NAD-ALDH

Once an alcohol has been oxidized to an aldehyde, a second class of enzymes has been found which can then oxidize the aldehydes to carboxylic acids. NAD-ALDH has also been purified from *S. cerevisiae*. The NAD-ALDH from baker's yeast has been shown to have the highest affinity for oxidizing acetaldehyde to acetic acid but also has the ability to oxidize other aldehydes at a much lower efficiency. The ALDH enzymes present in baker's yeast which have been identified have a molecular weight approximately between 50 and 60 kDa.[7]

ALDH1 has been crystallized and has dimensions of 9 x 6 x 4 nm comprised of two homo-monomers joined together to form a dimer. The size of ALDH agrees reasonably well with the approximation Eq. 2.1 which slightly over-approximates the diameter at 10 nm. While Eq. 2.1 does overestimate the diameter of enzyme, the calculation provides a valuable estimate since the majority of enzymes have not been crystallized and, as such, precise dimensions remain unknown. The ALDH enzyme requires NAD^+ or $NADP^+$ as a cofactor in the same manner as the ADH enzymes but also requires the presence of K^+ ions in order to be activated. The catalytic center of ALDH has been shown to be centered on the thiol of the cysteine subunit, which is located at the active region which is depicted in Figure 2.2 as a black asterisk. NAD-ALDH exhibits a narrow specificity for acetaldehyde. This specificity is due to the natural acetaldehyde presence from the oxidation of ethanol occurring at NAD-ADH.[8]

2.1.1.3 PQQ-ADH

Unlike ADH and ALDH purified from *S. cerevisiae*, the dehydrogenases which have been purified from G*luconobacter* are not NAD^+- or $NADP^+$-dependent. Instead the alcohols are oxidized at the PQQ structure bound within the quaternary enzyme structure. PQQ, the chemical structure of which can be found in Figure 2.3, acts as the active site for oxidation by reducing to $PQQH_2$ upon full reduction. The four heme structures present within the enzyme function as the electron acceptors which maintain electroneutrality during catalysis after the transfer of the negatively charged hydride.

PQQ-ADH is comprised of two distinct subunits resulting in a heterodimer. The first subunit is approximately 80 kDa and has both a heme b structure as well as PQQ forming the catalytic domain. The second subunit weighs 50 kDa and contains three heme c centers but lacks PQQ, and thus may contribute to higher turnover rates as an electron acceptor but is not classified as a catalytic region. *Gluconobacter* is a member of the acetic acid bacteria and are often found nearby ethanol fermentation sources such as decaying fruit. It is no surprise then that PQQ-ADH, much like NAD-ADH, also exhibits the highest activity for the oxidation of ethanol to acetaldehyde.[9,10]

2.1.1.4 PQQ-ALDH

PQQ-ALDH, much like the PQQ-ADH enzymes, is also comprised of two subunits with approximate masses of 80 kDa and 50 kDa, respectively. The larger subunit is comprised of a single PQQ and a heme b structure and is the catalytic domain of the enzyme. The smaller subunit contains three heme c groups but no PQQ has been identified. The second subunit, however, is key to the quaternary structure enabling the catalytic properties as neither subunit has displayed any oxidative catalytic activity on

their own.[11] Similar to the NAD-ALDH, the PQQ-dependent ALDH enzymes exhibit the greatest peak in activity for acetaldehyde, but are also capable of oxidizing formaldehyde and propionaldehyde to a lesser extent.[11]

2.1.1.5 FAD-GDH

GDH enzymes are widely studied due to their importance in healthcare applications of glucose monitoring for persons with diabetes.[12] In recent years, GDH has also gained popularity for use in biofuel cells due to the high activity values which provides high sensitivity to low fuel concentrations. GDH purified from certain fungus strains has been shown to be dependent on FAD as shown in Figure 2.4. Akin to the PQQ-dependent dehydrogenases, FAD is comprised of the quaternary structure of the enzyme. The FAD-GDH utilized in this paper was purified from *Aspergillus sp.* and while it has not yet been crystallized, the molecular weight has been approximated to 88-135 kDa.[13] FAD-GDH is extremely selective in the oxidation of D-glucose to D-glucono-1,5-lactone, with only limited activities to the oxidation of 2-deoxy-D-glucose and D-xylose and exhibits no activity towards other sugars.[14]

2.1.1.6 Laccase

Laccase is a multicopper containing enzyme which is found in a variety of flora and fungi species which catalyze the reduction of oxygen to water. Laccase purified from *Trametes versicolor,* a white rot fungus, has a molecular weight of 65 kDa and is a monomeric enzyme. It was utilized in this research as a biocathode for the catalytic reduction of oxygen.[15] Laccase from *Trametes versicolor* exhibits an activity maximum at pH 4. Although this activity maximum occurs under acidic conditions, laccase has

been shown to exhibit higher stability under alkaline conditions for long-term use, but activity is significantly reduced due to the high concentrations of OH^- which inhibit auto-oxidation.[16]

2.1.2 Enzyme Immobilization

Enzymes are able to be immobilized inside of metal organic frameworks through a variety of mechanisms. The mechanisms covered in this thesis are: π-π interactions, chemical bonding, and finally, encapsulation and confinement, which is also known as size selective sheltering. The primary concern for each of the aforementioned mechanisms is maintaining enzymatic activity after immobilization. In some cases, immobilization has resulted in an increase in enzyme activity and stability as has been previously mentioned. However, immobilization will often result in a decrease in activity.[17]

2.1.2.1 π-π Interactions

π-π interactions, also known as π stacking, of molecules refers to the noncovalent interactions between parallel p orbitals from molecules in close proximity. π stacking refers to the interaction between two planar molecules which experience a bonding force, which is at a distance such that the van der Waals force is negligible. The molecules arrange in a parallel fashion and slightly offset from one another such that the repulsive forces from the π orbitals are minimized. This allows the attractive forces of the neighboring molecule to exhibit a maximum attraction on the negatively charged π orbital of the first molecule. The resulting force has been calculated to be less than 10 kJ/mol, with the precise value dependent on the participating molecules.[18]

Benzene is the prototypical structure to exhibit π stacking at liquid nitrogen temperatures. Larger molecules, such as polyporphyrin which contain more atoms contributing to the planar structure, have a sufficient binding energy to maintain the interaction at or above room temperature. Large planar structured ligands, including those based on polyporphyrin derivatives, which are currently being developed in MOFs, provide promising developments for π stacking with enzymes.[19,20]

1-Pyrenebutanoic acid succinimidyl ester (PBSE), for example, has exhibited large enough of a binding energy to immobilize enzymes onto carbon nanotubes.[21] Immobilization occurs through π-π interactions between pyrene and carbon nanotubes. PBSE then immobilizes enzymes through a nucleophilic attack on the amine groups of an enzyme, as depicted in Figure 2.5. [22] The combination of noncovalent interaction along with the chemical bonding between PBSE and enzymes allows for a greater variety of enzymes which could be immobilized to planar MOF structures than simply those enzymes which are able to directly participate in π stacking.

2.1.2.2 Encapsulation and Confinement

Encapsulation and confinement are closely related mechanisms where the size ratio between the pore size of the MOF and the inclusion (enzyme) filling the void are the key distinction. Encapsulation occurs when the inclusion is of an equal or smaller diameter than the pore diameter but larger than the opening in the framework, known as a pore window. The mechanism of confinement, in comparison, is when the inclusion is larger than the pore volume but the crystal forms a distorted structure around the inclusion. Confinement is also referred to in research as size-selective sheltering.[23] If an inclusion, such as an enzyme, requires conformational changes in order to undergo the

catalytic reaction, confinement may inhibit this activity and be unsuitable for the desired application.

Since the enzyme is larger than the pore window for encapsulation, and simply larger than the pore volume for encapsulation, both encapsulation and confinement require the assembly of the MOF to occur with the enzymes to be present in solution during synthesis. This requires that synthesis of the MOF must occur under aqueous conditions with temperatures at or near room temperature. Temperature demands in particular for encapsulation and confinement require a balance of MOF growth and enzyme stability. MOF formation will occur more rapidly at higher temperatures. Enzymes, however, are more likely to denature the higher the temperature and, as such, the synthesis must be optimized.

2.1.2.3 Chemical Bonding

Finally, the last method of enzyme immobilization is chemical bonding, which encompasses both the crosslinking of enzymes as well as using linker molecules to chemically bind enzymes to the ligands. For MOF structures in which enzymes are smaller than the pore windows and do not exhibit π stacking, the chemical bonding of enzymes via sulfide bonds must be employed. Crosslinking can be used to create sulfide bonds between two enzymes in separate pores, or directly between the enzyme and the ligand of the MOF if the ligand has the appropriate chemical structure. Care must be taken in the selection of chemistry when chemically bonding to ensure that catalytic activity remains, as has been demonstrated in previous works.[24,25]

2.2 Experimental

2.2.1 Reagents

All chemicals and reagents unless specifically noted in the procedure were purchased from Sigma-Aldrich and used without further purification. The NAD-dependent enzymes were also purchased from Sigma-Aldrich and used as received. Both NAD-ADH and NAD-ALDH purchased were purified from *Saccharomyces cerevisiae*. The PQQ-dependent enzymes were purified from G*luconobacter* by Sidney Aquino Neto, a member of the Minteer group according to a previously reported procedure[26]. Due to the similarity of structures for the PQQ-ADH and PQQ-ALDH, as well as the ultimate goal of using both in an enzymatic cascade, the PQQ-dependent enzymes were not independently purified but rather left combined in solution. Finally, FAD-GDH was purchased and used as received from Sekisui Enzymes.

2.2.2 Procedures

2.2.2.1 π- π Interactions

When research initially began on this project, it had been recently reported that MP-11 had been successfully immobilized in Tb-meso MOF. At the time of reporting, the reason for immobilization was unknown. To test if Tb-meso MOF could immobilize other enzymes which are of interest in biofuel cells, NAD-ADH was substituted for MP-11 in the previously reported procedure to attempt immobilization.[17] The procedure is as follows; 1 mg of Tb-meso MOF and 1.75 mg NAD-ADH were added to a 1.5 mL low bind protein microcentrifuge tube. 1 mL of 100 mM HEPES buffer, pH of 7.5 was then added, and the mixture was allowed to incubate at 37 C for 2 days with the capped tube placed in a water bath to maintain temperature. After the 48 hours of incubation, the

supernatant was then drained, at which point the MOF crystals were then thoroughly rinsed with 18 MΩ-cm water to remove any free enzyme present.

The PQQ dependent enzymes were subsequently tested once the group which had initially reported the immobilization of MP-11 in Tb-meso MOF released a second report in which the heme of MP-11 had been showed to π stack with the two overlapping triazine rings from two TATB ligands.[27] The presence of four hemes in both the PQQ-ADH and PQQ-ALDH made these enzymes ideal candidates for immobilization. For enzyme immobilization, 1 mg of Tb-meso MOF and 25 µL of PQQ enzyme solution were added to a 1.5 mL low bind microcentrifuge tube. 1 mL of 50 mM phosphate buffer, ph 7.2 was then added to the tube which was then capped and placed into a water bath for 48 hours at 37 C. After 2 days, the supernatant solution was removed and the PQQ loaded MOF crystals were rinsed 10 times with 18 MΩ-cm water to remove any free enzyme.

The enzyme-loaded MOF crystals were then tested for the presence and concentration of enzyme loaded in or on the MOF. Enzyme concentration was determined using a bicinchoninic acid (BCA) assay, which is described in detail in the following section.

2.2.2.1.1 BCA Assay

As previously mentioned, enzyme concentrations within or adsorbed to the MOFs after thorough rinsing were determined using a BCA assay. The BCA assay consists of a two-part solution. The first contains BCA in buffer solution (Reagent A) and the second contains copper sulfate (Reagent B). The Cu^{2+} ions from dissolved copper sulfate are reduced to Cu^{+} by peptide bonds present in enzymes at 30 C to maintain a controlled reaction rate for 30 minutes. The reaction is then quenched by cooling the samples to 4 C

for 5 minutes. The BCA then coordinates to Cu^{+} which exhibits an absorption maximum at 562 nm (purple). [28] The samples are then analyzed using a UV-Vis spectrophotometer against a calibration curve of known concentrations which are prepared and analyzed at the same time as the unknown samples. One such calibration curve is depicted in Figure 2.6. A third order polynomial fit is used for the calibration to adequately represent concentrations from 100-2000 µg/mL. For analysis, a Pierce BCA kit was used which included prediluted enzyme standards with which to create the calibration curve. Unknown samples were carried out in triplicate to ascertain statistical significance of results.

First, in a 50 mL beaker, a solution of 50:1 v/v Reagent A to Reagent B was prepared at a volume of 2 mL/sample. For the standards provided, 100 µL of each concentration was pipetted into a 2.5 mL cuvette. 1 mg of enzyme loaded MOF was added to the cuvettes, in lieu of a volumetric quantity of free enzyme. 2 mL of reagent solution was then added to the cuvettes, which were promptly capped and inverted several times. The samples were then incubated in a water bath at 30 C for half an hour. After incubation, the samples were removed from the water bath and allowed to cool at 4 C for 5 minutes to stop the reaction. A UV-Vis spectrophotometer, set to read absorbance at 562 nm, was then used to record results.

The amount of enzyme per mass of MOF can then be calculated using Eq. 2.2, where L_m is the enzyme loading in the MOF, c is concentration calculated from the curve, v is the volume in the cuvette, and m is the mass of MOF. The loading of a MOF can be approximated according to Eq. 2.3, where the surface area of the enzymes present is compared to the surface area of the MOF. L_{SA} is the percent loading of enzymes in

comparison to surface area of MOF, m_{enz} is the mass of enzyme present, N_A is Avogadro's number, MW is molecular weight of the enzyme, SA_{enz} is the surface area of a single enzyme, m_{mof} is the mass of MOF which correlates to m_{enz}, and finally, SA_{MOF} is the specific surface area of the MOF. Eq. 2.3 assumes that the entire surface area of enzyme is in contact with available surface area of the MOF, meaning that all enzymes are assumed to be incorporated into pores and not surface adsorbed.

$$L_m\left(\frac{mg}{g}\right) = \frac{c\left(\frac{\mu g}{mL}\right) * v\ (mL)}{m\ (mg)} \qquad \text{(Eq. 2.2)}$$

$$L_{SA}\ (\%) = \frac{m_{enz}(g) * N_A\ (\frac{1}{mol})}{MW\ (\frac{g}{mol})} * \frac{SA_{enz}\ (cm^2)}{SA_{MOF}\left(\frac{cm^2}{g}\right) * m_{MOF}\ (g)} * 100 \qquad \text{(Eq. 2.3)}$$

2.2.2.1.2 NAD Activity Assay

Activity assays can also be utilized to determine the presence of enzymes and whether or not the immobilization technique used has altered or inhibited catalytic activity. The activity of NAD enzymes was always tested using this procedure. The following describes the procedure with Zn MOF-74 as the exemplary MOF. 10 mg of MOF/74-t of 88, 166, and 240 hours each had 5 mg of NAD-ADH along with 5 mL of 18 MΩ-cm ultrapure water added to a 10 mL vial and allowed to sit for 1 hour at room temperature to allow intercalation of the enzymes into the MOF. The MOF crystals were then rinsed repeatedly in 18 MΩ-cm water to remove any free enzyme. The crystals were then tested using an enzymatic activity assay to attempt to discern if loading had occurred. The activity assay for NAD-ADH was followed according to the manufacturer's specifications which are detailed below.

NAD-ADH oxidizes alcohols, with a strong affinity of the oxidation of ethanol with the reductive cofactor of NAD^+ to NADH. The procedure for optimal enzymatic

activity as described by Sigma-Aldrich is as follows.[29] A final volume of 2.0 mL were added to a 2.5 mL cuvette for analysis using a UV-Vis spectrophotometer monitoring the change in adsorption at 340 nm, which is where NADH presents an absorptive peak. Final concentrations resulted in 22 mM sodium pyrophosphate buffer, pH 8.8, and 7.5 mM NAD^+ (freshly prepared) as well as 3.2% (v/v) ethanol. To this solution, 1 mg of NAD enzyme-loaded MOF was added in lieu of enzyme in solution. The MOF was then allowed to settle for 5 minutes prior to monitoring the change in absorbance. The samples were then monitored for 30 minutes at an interval of 5 minutes. The lengthy monitoring periods were to combat the diffusion limitations presented by the MOF crystals all present at the bottom of the cuvette, as opposed to enzymes in solution. A blank sample must also be analyzed to correct for NAD^+ which is reduced to NADH through non-catalytic pathways.

$$\text{Activity (U/mg)} = \frac{(\Delta A_{sample} - \Delta A_{blank})(vol)}{(M)(EC)} \qquad \text{(Eq. 2.4)}$$

The activity of enzymes can then be calculated using Eq. 2.4, the result is presented in units of activity per mass of MOF, rather than the mass of enzymes as is typically reported since the amount of enzyme present is unknown, unless previously calculated via other means such as BCA assay. For Eq. 2.4, vol is the total volume analyzed in the cuvette in milliliters, M is the mass of enzyme loaded MOF in milligrams, and EC is the millimolar extinction coefficient of the absorbing species.

2.2.2.1.3 PMS/DCPIP Activity Assay

For the PQQ-dependent and FAD-dependent enzymes, spectroscopic activity assays were conducted with the enzymes oxidizing the fuel and maintaining electroneutrality through the reduction of 2,6-dichlorophenol indophenol (DCPIP) which

is optically blue when in a neutral state. DCPIP then turns optically clear upon reduction. Phenazine methosulfate (PMS) is added to the solution to facilitate electron transport between the enzymes and DCPIP. The procedure for the assay is as follows:

PMS has an absorbance maximum at 600 nm (yellow) which will be present once full reduction of DCPIP has occurred, which is used as the reference spectra to measure the absorbance against. To set blank absorbance, 1.5 mL of 50 mM phosphate buffer, pH 7.3 and 200 µL of 600 µM PMS are added to a 2.5 mL cuvette and absorbance is measured at 600 nm. Samples include the buffer and PMS in the same manner as the absorbance blank with the addition of 100 µL of 700 µM DCPIP and 200 µL of 200 mM substrate, either ethanol or glucose for PQQ-ADH or FAD-GDH, respectively. Enzyme or enzyme-loaded MOF was then added and decrease in absorbance in measured over time. Blank samples without enzyme or enzyme-loaded MOF must be conducted in the same manner as samples to correct for any noncatalytic reduction of DCPIP in solution during analysis. Activity is then calculated using Eq. 2.4 in the same manner as the NAD activity assay as described in Section 2.2.2.1.2.

2.2.2.2 PBSE Immobilization

In order to combine the benefits of noncovalent interaction of π stacking with the broad selectivity of chemical binding, PBSE, the structure of which can be seen in Figure 2.7, was selected to attach to MOF structures, which in turn has the ability to immobilize enzymes via the succinimide dissociating from the rest of the molecule, allowing the carboxylate to participate in a nucleophilic to amine groups in the enzyme. PBSE has limited solubility in both methanol and DMF and both solvents were used. π stacking has been shown to be heavily dependent on solvent interactions.[30] With PBSE dissolved in

both highly polar methanol and mildly polar DMF can attempt to optimize the interactions.

For PBSE immobilization, the same procedure was followed whether PBSE was dissolved in methanol or DMF; however, the concentrations were varied due to the solubility of PBSE in the respective solvents. In a 10 mL beaker, PBSE was dissolved in either 1 mM methanol[22], or 10 mM DMF[21]. 10 mg of MOF was then added to the solution and allowed to sit at room temperature for 3 hours. Here MOF denotes both Zn MOF-74 as well as Cu BPTC MOF which were both independently tested. After 3 hours, the MOF was separated through filtration and was thoroughly rinsed with methanol or DMF, respectively, to remove any unbound PBSE. Presence of PBSE was then determined using a UV-Vis spectrophotometer. Pyrene absorbs at 340 nm and fluoresces at 376 nm, which persists upon π stacking.

2.2.2.3 Size Selective Sheltering

Due to the fact that many of the MOF structures which have been identified up to this point still have pore sizes which are smaller than many of the large complex enzymes which would be useful for biofuel cells, size selective sheltering provides a unique alternative to immobilize enzyme which are much larger than the pore volumes. Due to the mild synthesis conditions present for synthesis of ZIF-90, it is possible to dissolve enzymes into the aqueous solution. The procedure for synthesis was followed as described in Section 1.3.4 with the following modifications. After dissolving the ICA and polyvinylpyrrolidone (PVP), 40,000 molecular weight average, in ultra-pure water but prior to adding the zinc solution, enzyme was added. PVP was used as a capping agent to prevent the formation of excessively large crystal structures which would inhibit electron

transport during electrocatalysis. For the NAD-dependent enzymes, 12.5 mg of both NAD-ADH and NAD-ALDH were dissolved and allowed to stir for 5 minutes. For the PQQ-dependent enzymes, 25 µL of enzyme solution was added and allowed to stir for 5 minutes. The zinc solution was then added and the procedure outlined in Section 1.3.4 was followed. The rinsed crystals were then analyzed for enzyme concentration via BCA assay.

2.3 Results and Discussion

Tb-meso MOF loaded with NAD-dependent enzymes leached after only two rinses with ultra-pure water. This rapid leaching of enzymes is indicative that only weak surface adsorption occurred and no immobilization took place, likely due to the fact that unlike PQQ-dependent enzymes, the NAD-dependent enzymes lack a large planar subunit such as a heme. The PQQ-dependent enzymes, however, did not leach from Tb-meso MOF and were shown to have a constant enzyme loading of 2.2 %, or 19 ± 4 mg/g, as calculated using Eq. 2.2. This loading remained constant between four and ten rinses with ultra-pure water and the supernatant tested after rinsing through BCA assay did not reveal any enzyme leaching. This result shows that π stacking with hemes and the triazine rings in TATB also occurs with the PQQ-dependent dehydrogenases, as was suggested in the previously reported literature with MP-11[27]. The combination of the PQQ enzymes having a total volume approximately twice the pore volume and the low calculated enzyme loading of the MOF suggests that the enzymes are only able to immobilize at the surface of the MOF and not inside the pores.

Due to the low enzymatic loading which was able to be achieved in Tb-meso MOF, other frameworks were investigated. As previous research had demonstrated, the

formation of mesoporous Zn MOF-74 could be achieved through excess solvation for extended periods of time.[31] This research has also demonstrated that the same characteristic drop in XRD intensity, which corresponds to an increase in amorphous character, as previously reported can be achieved without the use excess solvation, as shown in Figure 2.8. All samples were scanned from 10 to 100 degrees 2θ, at a rate of 0.1 degrees per second to ensure valid comparative analysis.

Zn MOF-74 was chosen as a possible framework due to the electricochemically active zinc ions present throughout the framework as a possible means for immobilization.[32] However, since the zinc ions are electrically active, Zn MOF-74 is unsuitable for BCA assays as the active zinc ions reduced the Cu^{2+}. While the zinc ions were capable of reducing species such as Cu^{2+} in BCA assays, the zinc ions were shown to be incapable of oxidizing either ethanol or acetaldehyde as well as being unable to reduce NAD^{+}, which allowed for spectroscopic analysis of enzymatic activity using the NAD dependent enzymes.

For Zn MOF-74, no activity was observed as the absorbance change was identical for samples loaded with enzyme as to the controls of unloaded MOF. While an activity assay alone cannot disprove the presence of enzymes, the lack of activity is a strong indication and as such alternate immobilization methods were sought out. As a second means of immobilization, previous research has shown that 1-pyrenebutanoic acid succinimidyl ester (PBSE) is capable of immobilizing onto a planar structure such as carbon nanotubes and then complete a nucleophilic attack on an enzyme, thereby immobilizing the enzyme.[22]

While Zn MOF-74 is not a planar MOF, rather it exhibits a paddlewheel type structure, the large planar structure of pyrene in PBSE was tested to see if sufficient interaction between the zinc ions in the Zn MOF-74 and pyrene was present for immobilization. The presence of PBSE can be confirmed by fluorescence of pyrene which has a peak absorbance at 340 nm and an emissive peak at 376 nm with the use of a UV-Vis spectrophotometer. Zn MOF-74 crystals were tested after attempted loading of PBSE, but no fluorescence was noted. The lack of fluorescence indicated PBSE and Zn MOF-74 did not present sufficient bonding interaction for immobilization.

Zn MOF-74 was shown to lack a sufficiently planar structure to adsorb PBSE through π stacking. The zinc ions while electrochemically active, also did not contribute towards PBSE immobilization. Next, a more planar MOF was selected and studied for PBSE attachment. Unlike Zn MOF-74, the Cu BPTC MOF has fully coordinated metal ions; therefore, no interaction between the PBSE and the Cu^{2+} ions in the MOF structure was expected. The structure of Cu BPTC also exhibits a more planar structure as described in Section 1.2.3. Fluorescence testing again showed no presence of PBSE. From this testing, it was determined that a MOF structure must be significantly planar or present a much stronger π-π interaction as was present in Tb-meso MOF with the heme like structure for the use of PBSE immobilization. The large heme like structure of MMCF-2 presented as a likely candidate for π stacking of both the PQQ-dependent enzymes as well as PBSE for NAD-dependent enzyme immobilization. However, due to the inability to reproduce the MOF, these hypotheses were unable to be tested.

With the lack of success of immobilizing enzymes, a recently reported journal article described the size-selective sheltering of MOFs through a water-based synthesis in

which both the MOF precursors and enzymes could be present.[23] By having the enzymes present as the nucleated MOFs joined together to form larger and larger crystal domains, the enzymes would become trapped within the MOF even though the pore size of ZIF-90 is much smaller than that of the enzyme being entrapped. It was also shown that this size-selective sheltering of catalase improved the stability of the enzyme.[23] However, it must be noted that size-selective sheltering of some enzymes could inhibit activity depending on the conformational changes which must occur in order for catalysis to occur.[23]

The previously reported procedure was followed for encapsulating the NAD-dependent enzymes as they were commercially available and in a lyophilized form. In short, 25 mg of enzyme was added to the ZIF-90 procedure described in Chapter 1. Both NAD-ADH and NAD-ALDH were sheltered in the analysis and the concentrations were analyzed using BCA analysis, resulting in 220 ± 100 mg/g of MOF. The large error is due in part to the noise of spectroscopic analysis due to the fact that a portion of the nanoscopic MOF crystals remain dispersed in the solution, rather than settled, resulting in light scattering during analysis. Controls were completed to show that ZIF-90 did not directly affect the BCA analysis. Activity assays were then completed according to the manufacturer's specifications as described previously.

Activity of NAD-ADH was completed according to the procedure described in Section 2.2.2.1.2. NAD-ALDH, however, is reported to exhibit optimal activity in the presence of acetaldehyde under the conditions reported by Sigma-Aldrich.[33] All samples were analyzed using a UV-Vis spectrophotometer at a wavelength of 340 nm to measure the drop in absorbance as NAD is reduced to NADH. The final volume of solution is 2.0 mL and the final concentrations of solutions used were: 103 mM Tris buffer, pH 8.0, 0.67

mM NAD, 100 mM potassium chloride, 10 mM 2-mercaptoethanol, and 2 mM acetaldehyde. As was previously completed with the NAD-ADH, 1 mg of ALDH loaded MOF was placed into the cuvette prior to analysis and allowed to settle for 5 minutes. However, after 30 minutes of observation, no activity was observed when sheltered for either NAD-ADH or NAD-ALDH. It may be likely that, as previously mentioned, the necessary conformational changes were restricted preventing catalysis.

After the NAD-dependent enzymes had been eliminated as possible candidates for the size-selective sheltering of ZIF-90, the PQQ-dependent enzymes were then analyzed. The PQQ-dependent enzymes were purified from Sidney Neto Aquino, a member of the Minteer lab. The ultimate goal has been to create enzymatic cascades and, as such, the ADH and ALDH enzymes were not independently purified. The PQQ enzymes were purified to a concentration of 10 mg/mL and exhibited a free enzyme activity of 5 U/mL at the time of analysis. BCA analysis of the loaded ZIF resulted in 160 ± 25 mg/g of enzyme loaded in the MOF which corresponds to approximately 4% loading of total surface area.

As in the NAD-dependent enzymes, the PQQ-dependent enzymes were also initially tested using a UV-Vis spectrophotometer using a 2.5 mL cuvette filled to a final volume of 2.0 mL. Activity assays for PQQ-dependent enzymes were completed with 1.5 mL of 50 mM phosphate buffer, pH 7.3 as well as 200 µL of 70 µM phenazine methosulfate (PMS) which is used as an electron mediator. PMS has an optical absorption maximum at 600 nm (yellow) which is set as the zero of absorbance. 100 µL of a 700 mM 2,6-dichlorophenol indophenol (DCPIP) solution as the reductive species is then added. DCPIP is deep blue in color prior to reduction, which then becomes

optically clear in its reduced state. Finally, 1 mg of PQQ-loaded MOF is then added and allowed to settle for 5 minutes. Once the enzyme is in presence of the fuel, in this case either ethanol or acetaldehyde, the oxidation of the fuel will result in the DCPIP being reduced and a decrease in absorption from the initially dark blue coloring. The PQQ loaded MOF was shown to have an activity of 0.40 ± 0.15 U/mg with ethanol as the initial fuel, as calculated using Eq. 2.4. While the enzyme loaded into ZIF-90 presents an order of magnitude lower activity than that of the free enzyme, the diffusion limitations of the encapsulated enzymes in such a spectroscopic assay overstate the reduction in activity.

2.4 Conclusions

In closing, two MOFs were able to successfully immobilize alcohol and aldehyde dehydrogenases. The first was Tb-meso MOF which was able to immobilize small quantities of the PQQ-dependent dehydrogenases through π stacking. The limited enzymatic loading of Tb-meso MOF proved to be insufficient for electrocatalysis, as will be discussed in more detail in Chapter 3. The attempts to immobilize enzymes using Zn MOF-74 and Cu BPTC MOF were unsuccessful despite multiple attempts and using secondary immobilization techniques such as PBSE. Finally, size-selective sheltering of enzymes within ZIF-90 was shown to be an effective mode of immobilization for the PQQ-dependent enzymes. The NAD-dependent enzymes did not exhibit any activity once sheltered. One possible cause for the lack of activity in the NAD-dependent enzymes is the inhibition of conformational changes upon immobilization through size selective sheltering. The PQQ-dependent enzymes did not lose activity, though activity in solution was an order of magnitude lower once immobilized compared to free enzymes.

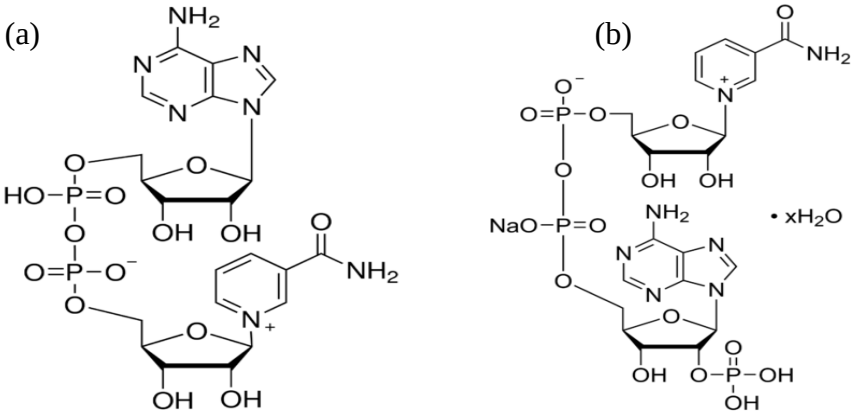

Figure 2.1: Chemical structure of NAD (a) and NADP (b)

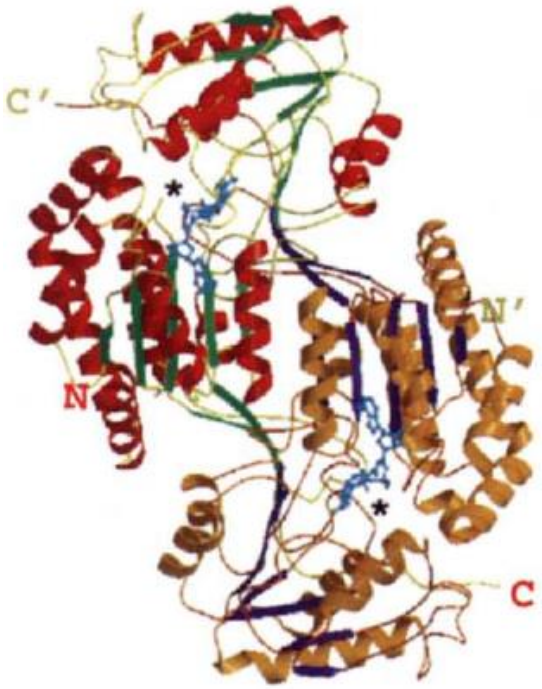

Figure 2.2: ALDH structure exhibited with monomer A colored in red and green, monomer B displayed in blue and gold. Reprinted with permission from [8]. Copyright (1997) Nature Structural and Molecular Biology.

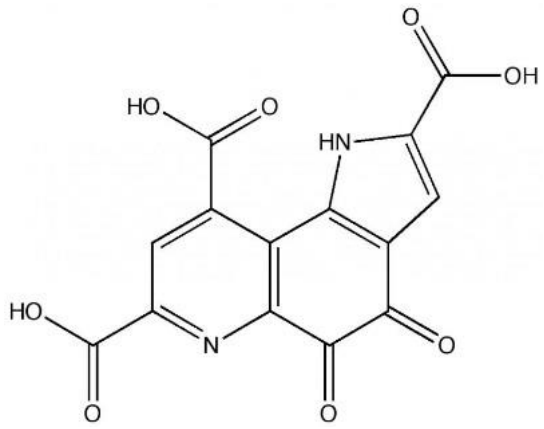

Figure 2.3: Chemical structure of PQQ

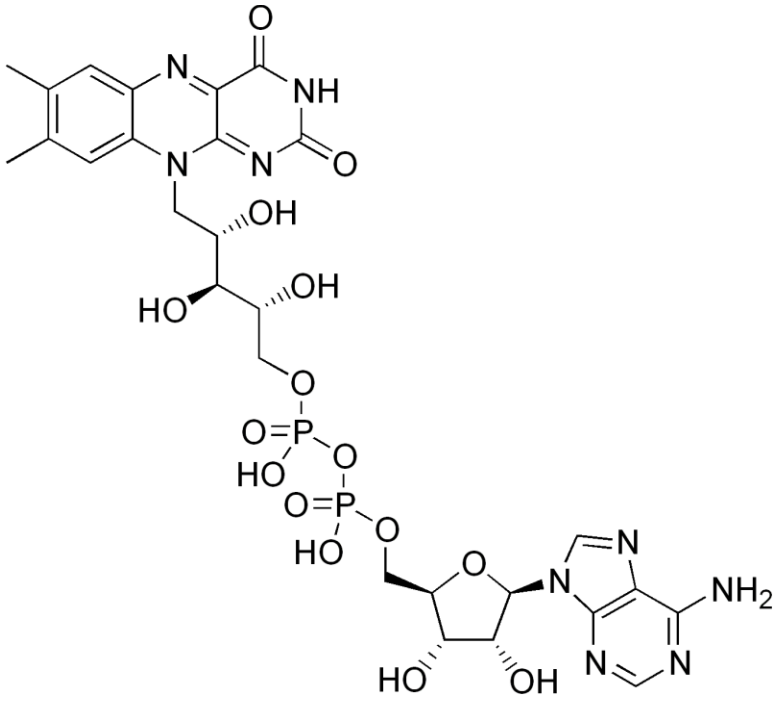

Figure 2.4: FAD chemical structure

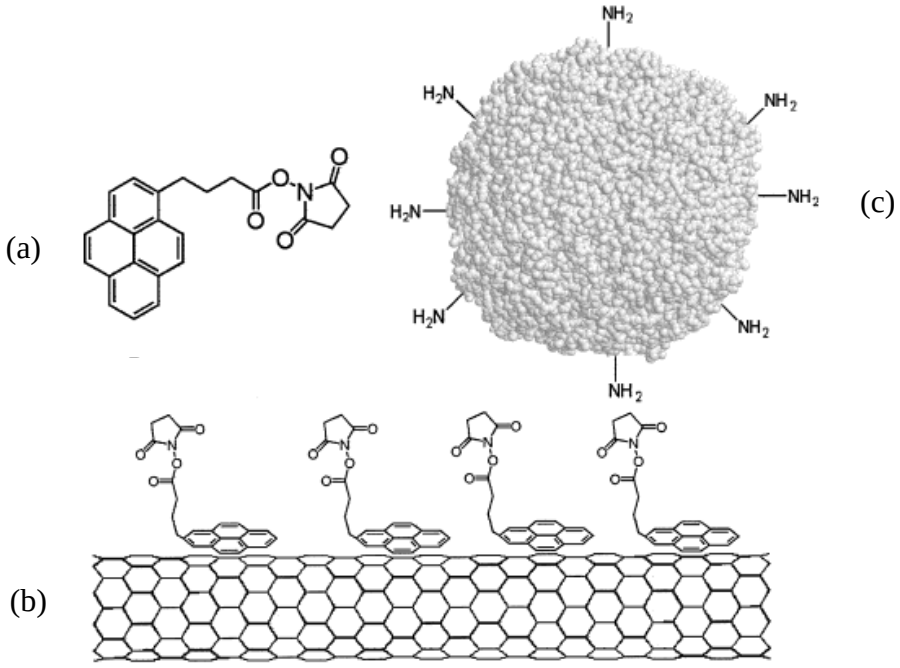

Figure 2.5: Depiction of PBSE (a) π stacking mechanism to carbon nanotubes (b) and amine groups on enzyme (c) where nucleophilic attack takes place. Reprinted with permission from [18]. Copyright (2001) American Chemical Society.

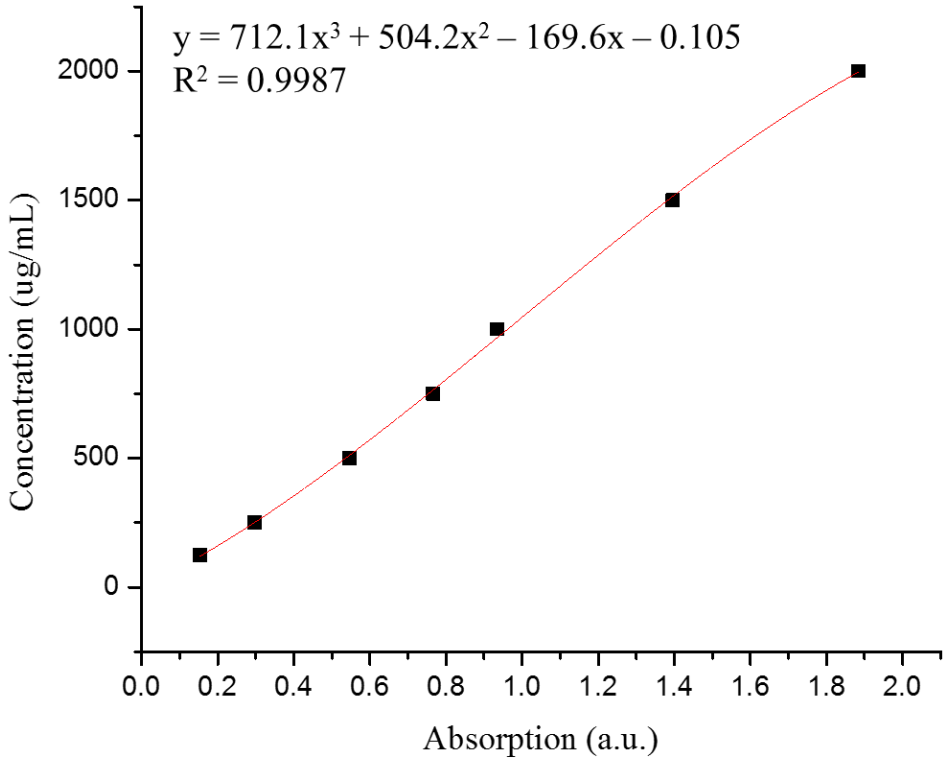

Figure 2.6: BCA calibration curve used for quantification of Tb-meso MOF loaded with PQQ-ADH

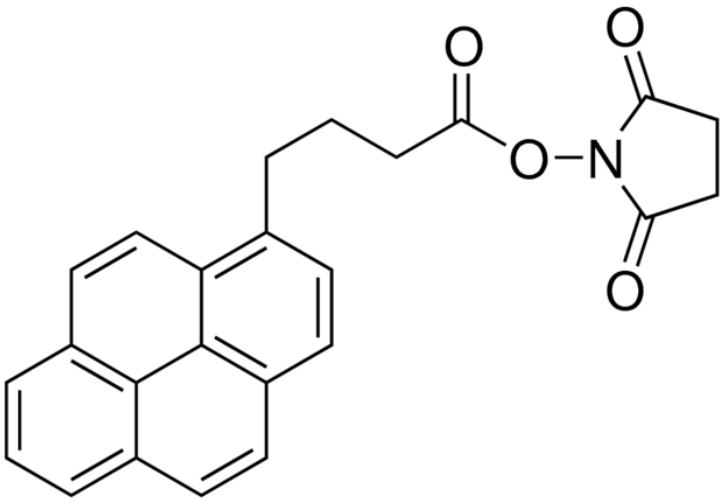

Figure 2.7: Chemical structure of PBSE

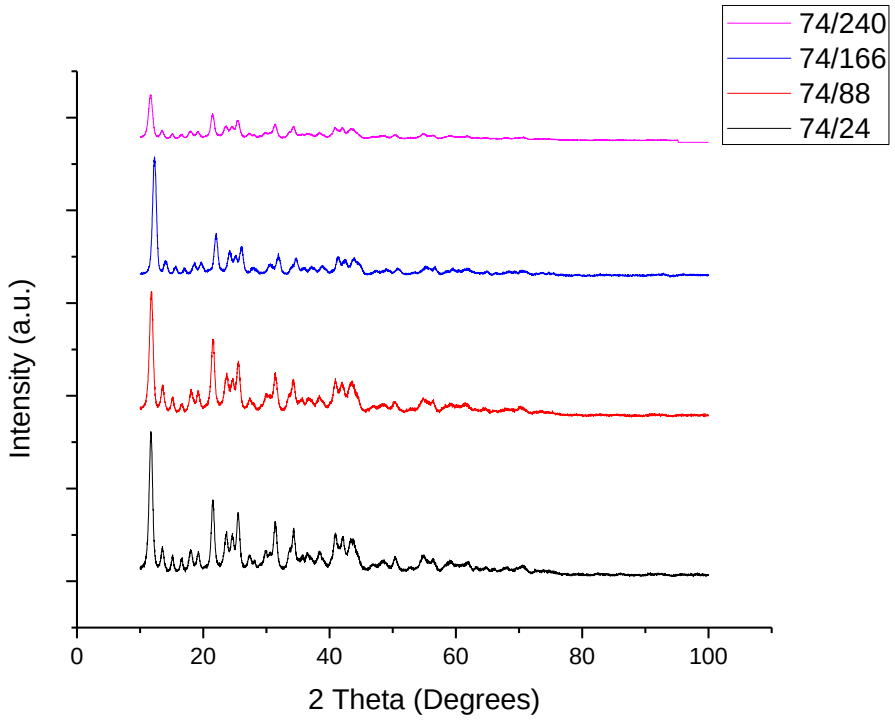

Figure 2.8: XRD patterns for Zn MOF-74/t where t is in hours.

2.5 References

(1) Beese, L. S.; Steitz, T. A. In *Nucleic Acids and Molecular Biology*; Eckstein, P. D. F., Lilley, D. D. M. J., Eds.; Nucleic Acids and Molecular Biology; Springer Berlin Heidelberg, 1989; pp 28–43.

(2) Jacobo-Molina, A.; Ding, J.; Nanni, R. G.; Clark, A. D.; Lu, X.; Tantillo, C.; Williams, R. L.; Kamer, G.; Ferris, A. L.; Clark, P. *Proc. Natl. Acad. Sci.* **1993**, *90* (13), 6320–6324.

(3) Protein | biochemistry :: The specificity of enzymes http://www.britannica.com/EBchecked/topic/479680/protein/72589/The-specificity-of-enzymes (accessed Jun 10, 2015).

(4) Erickson, H. P. *Biol. Proced. Online* **2009**, *11* (1), 32–51.

(5) Nobbmann, U. Protein sizing by light scattering, molecular weight and polydispersity.

(6) De Smidt, O.; du Preez, J. C.; Albertyn, J. *FEMS Yeast Res.* **2008**, *8* (7), 967–978.

(7) Wang, X.; Mann, C. J.; Bai, Y.; Ni, L.; Weiner, H. *J. Bacteriol.* **1998**, *180* (4), 822–830.

(8) Liu, Z.-J.; Sun, Y.-J.; Rose, J.; Chung, Y.-J.; Hsiao, C.-D.; Chang, W.-R.; Kuo, I.; Perozich, J.; Lindahl, R.; Hempel, J.; Wang, B.-C. *Nat. Struct. Biol.* **1997**, *4* (4), 317–326.

(9) Razumiene, J.; Niculescu, M.; Ramanavicius, A.; Laurinavicius, V.; Csoeregi, E. *Electroanalysis* **2002**, *14* (1), 43.

(10) Yakushi, T.; Matsushita, K. *Appl. Microbiol. Biotechnol.* **2010**, *86* (5), 1257–1265.

(11) Gomez-Manzo, S.; Chavez-Pacheco, J. L.; Contreras-Zentella, M.; Sosa-Torres, M. E.; Arreguin-Espinosa, R.; Perez de la Mora, M.; Membrillo-Hernandez, J.; Escamilla, J. E. *J. Bacteriol.* **2010**, *192* (21), 5718–5724.

(12) Yamaoka, H.; Sode, K. *J. Diabetes Sci. Technol. Online* **2007**, *1* (1), 28–35.

(13) Milton, R. D.; Lim, K.; Hickey, D. P.; Minteer, S. D. *Bioelectrochemistry* **2015**.

(14) Rodbard, D. In *Methods of protein separation*; Springer, 1976; pp 181–218.

(15) Patricia Zapata-Castillo. *Afr. J. Biotechnol.* **2012**, *11* (15).

(16) Stoilova, I.; Krastanov, A.; Stanchev, V. *Adv. Biosci. Biotechnol.* **2010**, *01* (03), 208–215.

(17) Lykourinou, V.; Chen, Y.; Wang, X.-S.; Meng, L.; Hoang, T.; Ming, L.-J.; Musselman, R. L.; Ma, S. *J. Am. Chem. Soc.* **2011**, *133* (27), 10382–10385.

(18) Hunter, C. A.; Sanders, J. K. M. *J. Am. Chem. Soc.* **1990**, *112* (14), 5525–5534.

(19) Gao, W.-Y.; Niu, Y.; Chen, Y.; Wojtas, L.; Cai, J.; Chen, Y.-S.; Ma, S. *CrystEngComm* **2012**, *14* (19), 6115.

(20) Gao, W.-Y.; Chen, Y.; Niu, Y.; Williams, K.; Cash, L.; Perez, P. J.; Wojtas, L.; Cai, J.; Chen, Y.-S.; Ma, S. *Angew. Chem. Int. Ed.* **2014**, *53* (10), 2615–2619.

(21) Ramasamy, R. P.; Luckarift, H. R.; Ivnitski, D. M.; Atanassov, P. B.; Johnson, G. R. *Chem. Commun.* **2010**, *46* (33), 6045–6047.

(22) Chen, R. J.; Zhang, Y.; Wang, D.; Dai, H. *J. Am. Chem. Soc.* **2001**, *123* (16), 3838–3839.

(23) Shieh, F.-K.; Wang, S.-C.; Yen, C.-I.; Wu, C.-C.; Dutta, S.; Chou, L.-Y.; Morabito, J. V.; Hu, P.; Hsu, M.-H.; Wu, K. C.-W.; Tsung, C.-K. *J. Am. Chem. Soc.* **2015**, *137* (13), 4276–4279.

(24) Wang, X.; Makal, T. A.; Zhou, H.-C. *Aust. J. Chem.* **2014**, *67* (11), 1629–1631.

(25) Tran, D. N.; Balkus, K. J. *ACS Catal.* **2011**, *1* (8), 956–968.

(26) Aquino Neto, S.; Hickey, D. P.; Milton, R. D.; De Andrade, A. R.; Minteer, S. D. *Biosens. Bioelectron.* **2015**, *72*, 247–254.

(27) Chen, Y.; Han, S.; Li, X.; Zhang, Z.; Ma, S. *Inorg. Chem.* **2014**, *53* (19), 10006–10008.

(28) Smith, P. K.; Krohn, R. I.; Hermanson, G. T.; Mallia, A. K.; Gartner, F. H.; Provenzano, M. D.; Fujimoto, E. K.; Goeke, N. M.; Olson, B. J.; Klenk, D. C. *Anal. Biochem.* **1985**, *150* (1), 76–85.

(29) Enzymatic Assay of Alcohol Dehydrogenase (EC 1.1.1.1) http://www.sigmaaldrich.com/technical-documents/protocols/biology/enzymatic-assay-of-alcohol-dehydrogenase.html (accessed Jun 4, 2015).

(30) Martinez, C. R.; Iverson, B. L. *Chem. Sci.* **2012**, *3* (7), 2191–2201.

(31) Yue, Y.; Qiao, Z.-A.; Fulvio, P. F.; Binder, A. J.; Tian, C.; Chen, J.; Nelson, K. M.; Zhu, X.; Dai, S. *J. Am. Chem. Soc.* **2013**, *135* (26), 9572–9575.

(32) Peterson, G. W.; Mahle, J.; Balboa, A.; Wagner, G.; Sewell, T.; Karwacki, C. J. *Evaluation of MOF-74, MOF-177, and ZIF-8 for the Removal of Toxic Industrial Chemicals*; DTIC Document, 2008.

(33) Enzymatic Assay of Aldehyde Dehydrogenase (EC 1.2.1.5) http://www.sigmaaldrich.com/life-science/metabolomics/enzyme-explorer/learning-center/assay-library.html (accessed Jun 4, 2015).

CHAPTER 3

BIOFUEL CELLS AND ELECTROCHEMISTRY

3.1 Introduction

3.1.1 Catalysis

Catalysts are instrumental in our daily lives. From reducing harmful pollutants in cars, to synthesizing industrial chemicals, pharmaceuticals, and even generating power, both the health and major sectors of our economy rely on catalysis. Catalytic reactions have been estimated to be a part of approximately 90% of all industrial processes.[1] Throughout the 20th century, catalysts largely fell into two categories: metal-based and homogenous organic catalysts. Since the turn of the 21st century, both governments and industries have begun to emphasize sustainable, or "green" chemistry, which has brought new focus on researching heterogeneous catalysts which are attempting to incorporate the reusability of metallic catalysts with the mild operating conditions of enzymatic catalysts. Anastas et al. have previously described the tenets of sustainable chemistry and how catalysis fits as one of, if not the key part in improving the atom economy and reducing waste streams while simultaneously increasing efficiencies.[2–4]

A catalyst is defined as an unconsumed species present during a reaction which facilitates an intermediary reaction between the initial and final products lowering the required activation energy and increasing the reaction rate simultaneously. A graphical view of this reduction in activation energy can be found in Figure 3.1. Where traditional

metallic catalysts can dramatically reduce the energetic requirements for a particular system, the operating conditions required are generally still quite hostile, requiring high temperatures and extreme pH, and often result in toxic byproducts. Recently, however, attention has been focused on using enzymatic catalysts in lieu of inorganic catalysts as a greener alternative.

Enzymatic catalysts are presently widely used in pharmaceutical and industrial applications due to their high specificity and mild operating conditions. Enzymes are currently introduced as homogenous catalysts into solution for these applications. However, this is impractical for fuel cell applications as the catalytic reaction needs to happen near the electrode surface if the electron is to participate in power generation. This requires the immobilization of the enzymes near the electrode surface for fuel cell applications. In addition, both enzyme stability and activity can be shown in some cases to be greatly increased through immobilization leading to more efficient and reusable catalysts.[5,6] Research on developing heterogeneous enzymatic catalysts immobilized within different frameworks is rapidly expanding, exploring a variety of materials including: porous silicates[7], zeolites[8], and more recently MOFs.[6,9–11]

3.1.2 Biofuel Cells

Fuel cells are devices which incorporate redox reactions at a cathode and anode which are separated by a membrane, which has selective ion permeability. An external load can then be placed between the anode and cathode, resulting in power generation. Biofuel cells are a subcategory of fuel cells in which biological entities such as microbes, enzymes, or cells facilitate the oxidation and reduction of the selected fuels as opposed to traditional fuel cells which rely on metallic catalysts. The first half cell reaction for

biofuel cells was demonstrated in 1911 by Potter, in which *Escherichia coli* were grown onto platinum electrodes which through the hydrolysis of simple starches and sugars generated electricity.[12] However, since the discovery showing that biological entities could be incorporated into fuel cells, the advancement in technology towards commercialization has been slow to be realized.

While enzymes afford the possibility to generate power through the oxidation of readily available fuels, such as methanol and ethanol under ambient conditions, removing the need for combustion-based generators in remote locations, significant challenges still remain. First, most enzymes in their biological settings will typically only survive for on a time scale of hours or days. For a viable commercial device, enzyme stability would need to be increased to months if not years. Enzyme immobilization has been shown in some cases to dramatically increase the stability of enzymes.[13] A second challenge present in biofuel cells is electron transport from the enzyme to the electrode surface. While a few enzymes have been able to show direct electron transfer (DET), such as multicopper oxidases[14], the majority of enzymes require a mediator in order to transport the electron from the catalytic center of the enzyme to the electrode surface, a process known as mediated electron transfer (MET).[15]

After demonstrating that ZIF-90 successfully sheltered the PQQ-dependent ADH and ALDH, the next step was to immobilize the enzyme-loaded MOFs onto an electrode to test viability for electricity generation in a half cell design. Two polymers were tested for viability as suitable membranes for MOF containment that would still allow the necessary diffusion of fuel into the enzymes. The first polymer tested was a Nafion polymer which had been modified with tetrabutylammonium bromide (TBAB) to

increase the porosity as well as neutralizing the acidic sulfonic groups, thereby enabling fuel transport from the bulk to the electrode surface where it could be oxidized by the enzymes. The TBAB-modified Nafion polymer is nonconductive and, as such, was testing whether or not the enzymes could participate in DET once contained within ZIF-90.

The second polymer employed was linear polyethylenimine dimethyl ferrocene (LPEI-DMFc) which enables MET through the ferrocene groups, which can self-exchange from the enzyme to the electrode. This polymer was designed to further probe the viability of PQQ-ADH and ALDH embedded into ZIF-90. After testing of PQQ-ADH and PQQ-ALDH, FAD-GDH was encapsulated within ZIF-90, herein noted as enzyme@MOF, as the activity of the enzyme is an order of magnitude larger than that of either PQQ-ADH or PQQ-ALDH.

FAD-GDH@ZIF-90 exhibited stability when drop cast onto the electrode and allowed to dry. Without the need of an additional polymer membrane, the diffusional resistance of the electrodes was significantly reduced. After catalytic activity was observed in half cell experiments, a full biofuel cell was then fabricated. FAD-GDH@ZIF-90 was drop cast onto a GCE acting as the bioanode. Laccase was immobilized onto Toray carbon paper with anthracene modified multiwalled carbon nanotubes (Ac-MWCNTs), for the reduction of oxygen to water acting as the biocathode, as has been reported from the Minteer research group previously.[16]

Ac-MWCNTs were used in order to facilitate DET by immobilizing laccase to the MWCNTs near the active site of the enzyme, as has been previously reported.[17] The fuel cell utilized was a membrane separated H-cell which is depicted in Figure 3.2. With the

use of an H-cell biofuel cell, both electrodes could operate under ideal pH conditions as FAD-GDH operating at the bioanode has optimal performance at a pH of 7, while laccase deposited on the biocathode has an activity peak at pH 4.

3.2 Experimental Procedures

3.2.1 Reagents

Ethyleneglycol diglycidylether (EGDGE) was purchased from Polysciences Inc. Nafion 100 EW, 5 wt % was purchased and used as received from Sigma-Aldrich All remaining reagents were of reagent grade and purchased from Sigma-Aldrich and were used as purchased without further purification.

3.2.2 Procedures

3.2.2.1 TBAB-modified Nafion Preparation

The preparation of TBAB-modified Nafion polymers to create porous hydrophobic polymer membranes have been previously reported from the Minteer research group.[18] The TBAB-modified Nafion polymer has been proven as an effective membrane for DET applications, but up until this point, no known research has tested its viability for enzymes bound within MOFs. Detailed instructions of creating the porous membrane can be found in the included references. The steps are described in brief in the following paragraphs.[18]

First, prepare a solution of Nafion with three times the molar equivalent of TBAB compared to that of the sulfonic groups present in the Nafion polymer. The solution is then vortexed for a minimum of 10 minutes to ensure adequate mixing. The solution is then pipetted into a thin layer in a plastic weigh boat and the volatiles are allowed to

evaporate overnight. The excess salts are then extracted by thorough soaking overnight in water followed by multiple rinses with 18 MΩ water to ensure all salts have been dissolved from the polymer. The polymer film is then allowed to dry overnight and is then re-dissolved in ethanol and vortexed for several hours until the suspension turns clear.[18,19]

Once the TBAB-modified Nafion polymer had been prepared, electrode preparation for cyclic voltammetry (CV) analysis was conducted. 0.071 cm^2 round glassy carbon electrodes (GCEs) were polished using a microfiber cloth and alumina particles which ranged in size from 1 µm down to 0.05 µm (Buehler). 1 mg of PQQ-ADH@ZIF-90 was then suspended in 5 µL ultrapure water and vortexed for 1 minute. Immediately after removing the suspension from the vortex, 4 µL was pipetted onto the electrode surface and was allowed to dry under vacuum at ambient temperature. Once dry, 5 µL of TBAB-modified Nafion was then pipetted on top of the MOFs to create the membrane. The electrodes were then dried under vacuum at ambient temperatures to limit the amount of time the enzymes were allowed to remain at room temperature prior to analysis.

3.2.2.2 LPEI-DMFc Preparation

The distance from the catalytic center of the enzymes to the electrode surface were likely too great once immobilized inside of ZIF-90 for DET to occur. As previously mentioned, the ferrocene side groups which have been modified to the LPEI polymer allow for high electron transport at a rate much greater than that of the enzymatic turnover rates. The polymer was synthesized by Dr. David Hickey, a postdoc in the Minteer research group and the synthesis of the polymer is described in a previously

reported paper which was followed with the following modifications.[20] The LPEI-DMFc polymer, the chemical structure of which can be found in Figure 3.3, is crosslinked using ethylene glycol diglycidyl ether (EGDGE). Due to the massive size of MOFs compared to enzymes which the polymer was originally developed to immobilize, the quantity of crosslinker was necessary to be optimized to prevent the peeling of the MOFs from the electrode surface.

It was found that 10 µL/45 µL EGDGE/H_2O provided the best stability and this was used for all conducted experiments. For electrode preparation, 0.5 mg of freshly prepared PQQ-ADH@ZIF-90 was suspended in 14 µL LPEI-DMFc solution and 0.75 µL EGDGE. The mixture was then vortexed for 2 minutes, at which point 4 µL was immediately pipetted onto the electrode surface. The polymer-MOF solution was allowed to cure for 24 hours to provide sufficient time for crosslinking to occur.

3.2.3 Bioanode Preparation

After failing to show catalytic activity with any of the ADH or ALDH enzymes on an electrode, FAD-GDH was chosen, as the activity of the enzyme was shown to be 625 ± 30 U/mg of enzyme, as compared to PQQ-ADH which was shown to exhibit an activity of 30 ± 5 U/mg in solution. FAD-GDH@ZIF-90 was suspended in 18 MΩ water at a concentration of 1 mg of MOF to 10 µL of water. This solution was then sonicated for 30 seconds followed by vortexing for 1 minute to ensure the solution was homogenous. 3 µL of the MOF solution was then pipetted onto a GCE, resulting in approximately 0.3 mg of FAD-GDH@ZIF-90 being drop cast onto the electrode which was allowed to dry under vacuum for 1 hour.

3.2.4 Biocathode Preparation

The laccase cathode was prepared following a procedure previously reported from the Minteer research group.[16] In brief, 1.5 mg of laccase was dissolved in 75 µL of a 0.2 M citrate/phosphate buffer at pH 4.0. To this solution, 7.5 mg of Ac-MWCNTs were added. This solution was then vortexed for 1 minute followed by sonication for 15 seconds. This regiment was repeated four times. 25 µL of TBAB-modified Nafion was then added, and one additional vortex and sonication cycle was completed. The solution was then painted onto three separate 1 cm^2 Toray carbon paper electrodes, resulting in approximately 33 µL per electrode. The electrodes were then dried under ambient conditions with forced air convection for 2 hours prior to analysis.

3.2.5 H-cell Design

The purpose of an H-cell biofuel cell is to optimize the pH conditions of both the bioanoe and biocathode such that each enzyme can operate in their ideal conditions. In order to prepare the membrane, Nafion 212 was cut into 1 in^2 squares and was stirred overnight in a 1 M H_2SO_4 in order to increase the conductivity of protons through the membrane. The anodic chamber was then filled with 150 mM sodium phosphate, and 1 mM NQSA as the electron mediator, at pH 7.2, while the biocathode chamber was filled using a 200 mM citrate/phosphate buffer, pH 4.0.

3.3 Results and Discussion

3.3.1 TBAB-modified Nafion Membrane

In order to test for catalytic activity of PQQ-ADH sheltered in ZIF-90 (PQQ-ADH@ZIF-90), cyclic voltammetry was completed from 0 V to 0.6 V vs. Ag/AgCl at a

scan rate of 0.01 V/s which should encompass the oxidative peak for the PQQ enzymes, beginning at approximately 0.3 V as has been previously reported, which is the oxidative peak for the heme c.[21] Electrodes were tested in a 0.2 M phosphate buffer, pH 7.4. Control samples of the electrodes prepared with BSA@ZIF-90 and TBAB-modified Nafion were first tested. Next, the PQQ-ADH@ZIF-90 loaded electrodes were tested without fuel as well as with 10 mM and 20 mM ethanol present. All scans were repeated six times in order to represent a stable signal. However, no catalytic activity was observed, and in fact, the heme c redox peaks could not be observed.

From these results, it was concluded that DET was not possible with PQQ-ADH@ZIF-90. As a result, a mediating polymer, LPEI-DMFc, was selected as the next materials candidate for MOF-electrode immobilization to test for MET bioelectrocatalysis. LPEI-DMFc was selected since the polymer is able to function as both the mediator as well as the structural membrane, ensuring that sufficient mediator will be in close proximity to both ZIF-90 and the electrode surface to facilitate electron transport.

3.3.2 LPEI-DMFc Membrane

Catalytic activity of PQQ-ADH@ZIF-90 was tested through cyclic voltammetry according to the following procedure. The prepared electrodes were placed in 0.2 M phosphate buffer, pH 7.4 and voltage was swept between 0 and 0.6 V, which exhibited the ferrocene cathodic and anodic peaks as expected which can be seen in Figure 3.4. Control samples of unloaded ZIF-90 were again tested and exhibited the same behavior. Ethanol was then added to the buffer. Concentrations of 5, 10, and 20 mM were initially tested, but no catalytic activity was observed.

A 50 mM ethanol solution was also tested but this high of a concentration led to the dissolution of LEPI-DMFc and subsequent delamination of the MOF from the electrode surface. After failing to show catalytic oxidation using CV, amperometry was next tested as the sensitivity is higher in amperometry than for CV. Voltage was set to 0.4 V vs. Ag/AgCl, once the current had stabilized. Ethanol was added in 2 mM intervals from 0 to 20 mM over a 30-minute period. However, amperometry was also unable to exhibit any catalytic activity for the system as no decrease in current was observed.

3.3.3 FAD-GDH@ZIF-90 Half Cell

FAD-GDH@ZIF-90 had shown catalytic activity through spectroscopic analysis. The next step necessary was to determine if the activity of the enzyme within the MOF was sufficiently large to be exhibited once deposited on an electrode. With 4% volumetric loading of FAD-GDH@ZIF-90, approximately 5 U of enzyme was deposited onto the electrode. Cyclic voltammetry and amperometry were conducted to determine catalytic activity. Catalytic activity was conducted using a buffer containing 100 mM sodium phosphate, 50 mM sodium nitrate and adjusted to pH 7.2, 1 mM of 1 2-naphthoquinone-4-sulfonic acid (NQSA) was added to act as the electron mediator. Control experiments were conducted with bovine serum albumin (BSA) encapsulated within ZIF-90 to confirm that there was no catalytic activity without FAD-GDH.

Catalytic oxidation began at approximately -80 mV vs. SCE with the oxidative peak at E_{an} = 20 mV. Figure 3.5 depicts the CV for FAD-GDH@ZIF-90 showing the lack of catalytic activity for the control samples of BSA@ZIF-90 and the catalytic response of FAD-GDH@ZIF-90 in the presence of 100 mM glucose and was shown to have an $E_{1/2}$ = 50 ± 10 mV. Amperometric analysis was next completed adding glucose in increments

of 10 mM until saturation occurred, as shown in Figure 3.6. The same buffer solution was used for CV, but the solution was stirred to eliminate diffusional limitations. By applying the Michaelis-Menten kinetics, as shown in Figure 3.6, it was calculated that FAD-GDH@ZIF-90 had a K_M = 20.3 ±4.1 mM glucose with a V_{max} = 41.3 ±1.2 μA/cm^2.

3.3.4 Biofuel Cell Characterization

The bioanode dropcast with FAD-GDH@ZIF-90 and the laccase painted biocathode were placed into the H-call biofuel cell described in Section 3.2. In order to complete control experiments, as in the half cell experiments, BSA@ZIF-90 was substituted for FAD-GDH@ZIF-90. Open circuit voltage (V_{OC}) for the blank samples prior to adding glucose was 659 ± 13 mV. After adding glucose, the V_{OC} shifted to 708 ± 16 mV. The control samples exhibited a V_{OC} of 654 ± 16 mV, confirming that no catalysis is present from the MOF framework in the absence of FAD-GDH in the presence of 100 mM glucose under hydrostatic conditions. The biofuel cell exhibited a maximum power density of 2.75 ± -0.40 μW/cm^2, as shown in Figure 3.7, which was shown to exhibit a V_{OC} of 708 ±16 mV and a short circuit current density (J_{SC}) of 4.46 ±54 μA/cm^2. Experiments conducted without glucose in FAD-GDH@ZIF-90 (blank) as well as control experiments of BSA@ZIF-90 in the presence of glucose (control) confirm the lack of catalytic activity, as can be seen in Figure 3.7, which fail to show catalytic power generation.

3.4 Conclusions

Catalytic activity was unable to be observed using either TBAB-modified Nafion or LPEI-DMFc membranes for MOF immobilization to the electrode surface with either

NAD-dependent of PQQ-dependent enzymes. However, this does not rule out the prospect of either being a viable membrane in the future. No response was noted for TBAB-modified Nafion which suggests that DET is not feasible with PQQ dehydrogenases loaded into ZIF-90 but cannot be definitively ruled out at this point due to a lack of signal through attempts of both DET and MET immobilization techniques.

For the LPEI-DMFc membrane, the small surface area available of the electrode coupled with the limited enzymatic loading of the MOFs combined to only having approximately 0.1 units of enzyme on the electrode. The redox peaks for ferrocene were readily displayed on CV, but no catalytic current was shown with either NAD or PQQ dependent ADH or ALDH. Due to the lack of activity present in immobilized ADH and ALDH, GDH was then encapsulated within ZIF-90 due to the relative high activity levels compared either NAD- or PQQ-dependent ADH and ALDH.

The performance of the glucose half-cell FAD-GDH@ZIF-90 anode exhibited stable catalytic activity even when stored at room temperature, with no discernible loss in catalytic activity after 2 weeks of storage with activity maintained at 625 ± 30 U/mg while free enzyme has activity of 900 ± 44 U/mg. Biocatalysis was shown to be present in the presence of glucose, with no catalytic activity being observed without glucose.

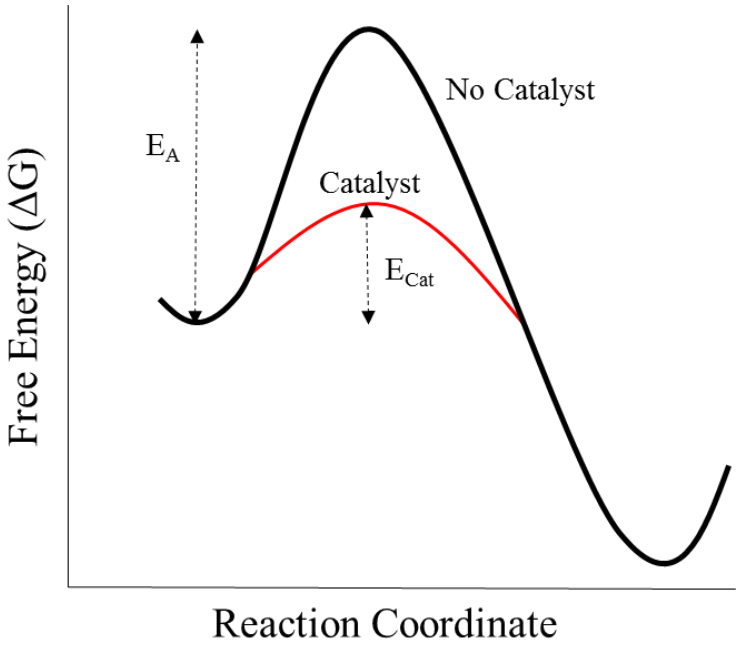

Figure 3.1: Depiction of activation energy with (E_{Cat}) and without (E_A) a catalyst

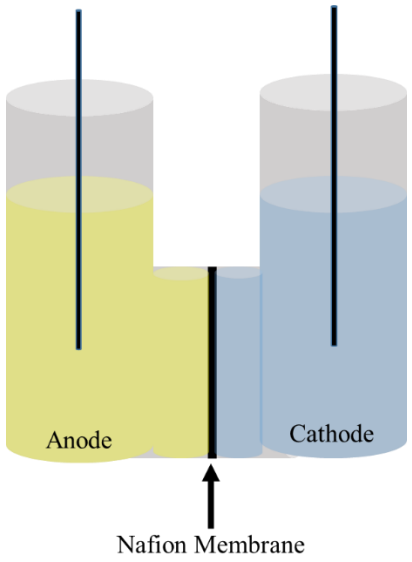

Figure 3.2: H-cell fuel design

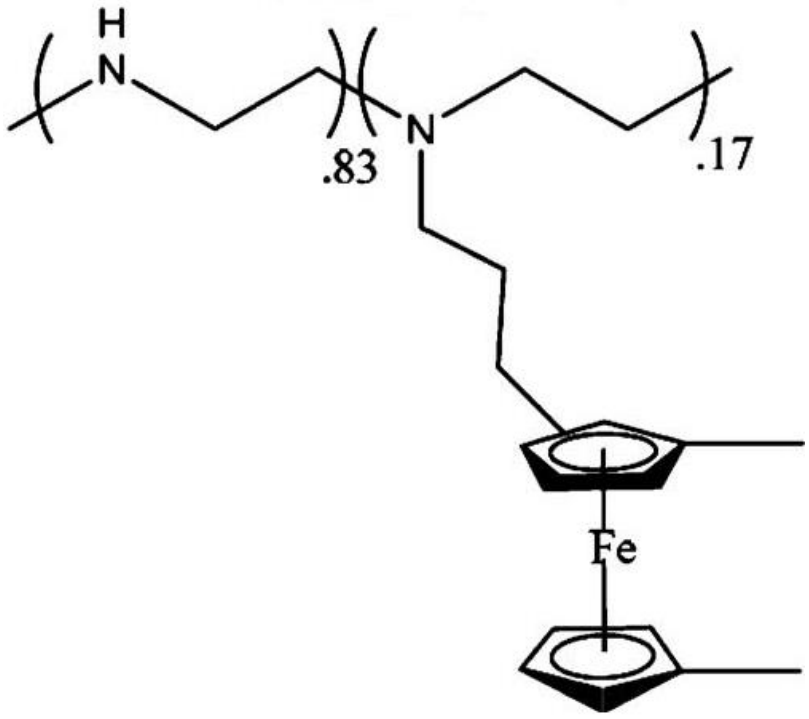

Figure 3.3: Chemical structure of LPEI-DMFc

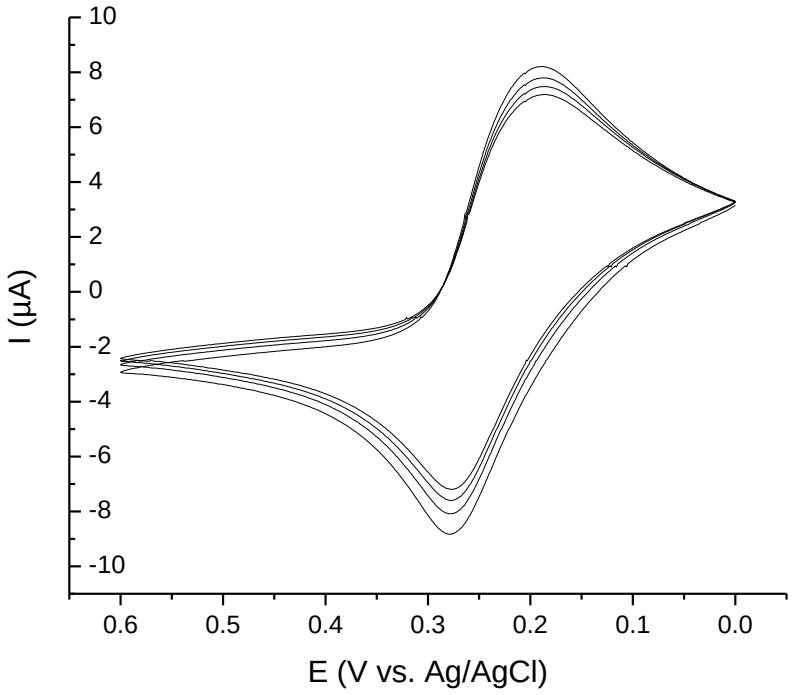

Figure 3.4: CV of PQQ-ADH@ZIF-90 immobilized on GCE using LPEI-DMFc membrane. 0.2 M phosphate buffer, pH 7.4

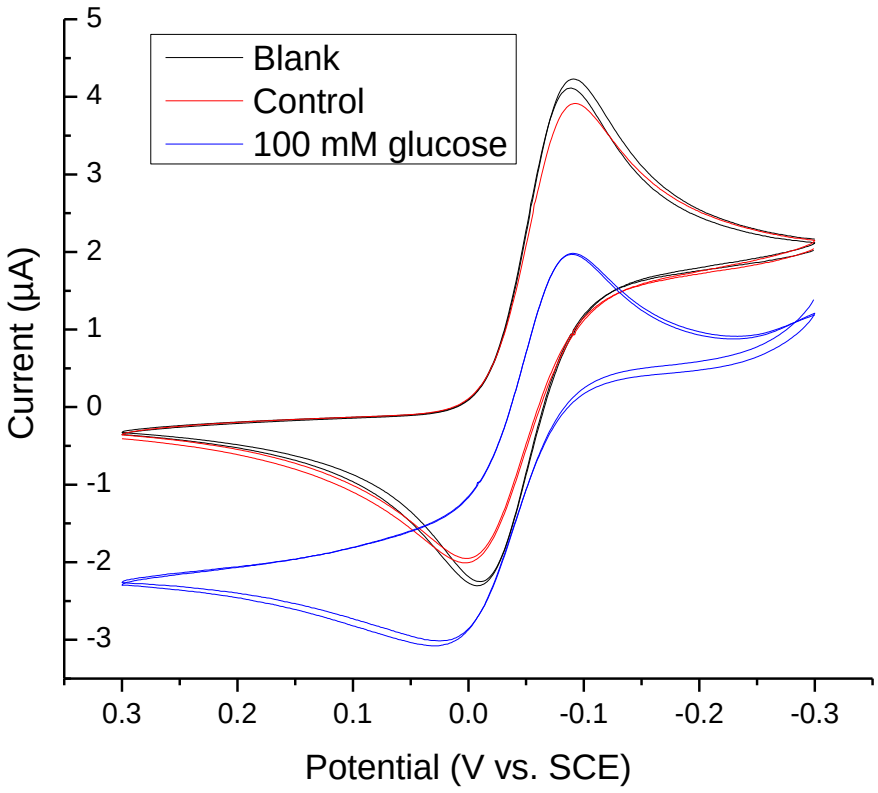

Figure 3.5: Cyclic voltammogram of FAD-GDH@ZIF-90 in 150 mM sodium phosphate buffer pH 7.2 with 1 mM NQSA. Blank is FAD-GDH@ZIF-90 in buffer. Control is BSA@ZIF-90 in presence of 100 mM glucose. Blue curve exhibits catalytic activity of FAD-GDH in presence of 100 mM glucose.

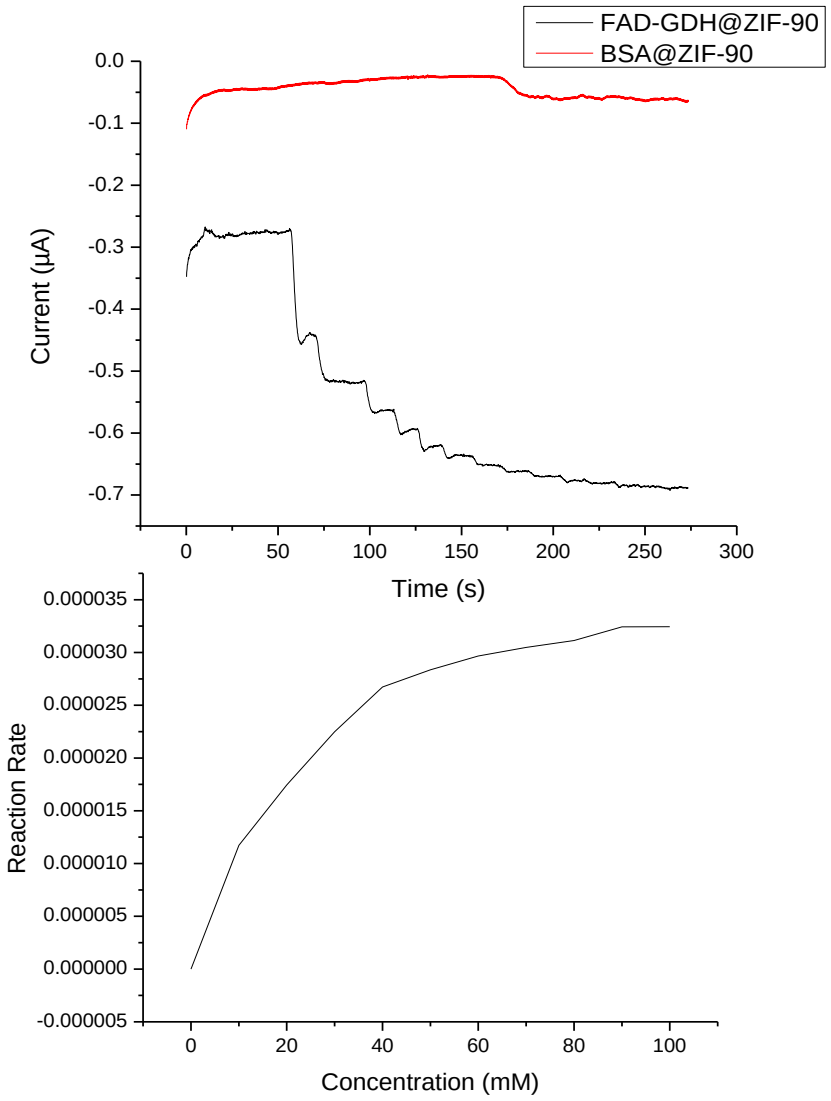

Figure 3.6: Amperometric results for half-cell reaction. Top: Amperomtery in 150 mM sodium phosphate buffer pH 7.2, 1 mM NQSA in 10 mM glucose additions up to 100 mM. Black curve is FAD-GDH@ZIF-90. Red curve is BSA@ZIF-90 as control. Bottom: Resulting Michaelis Menten plot from amperometry data

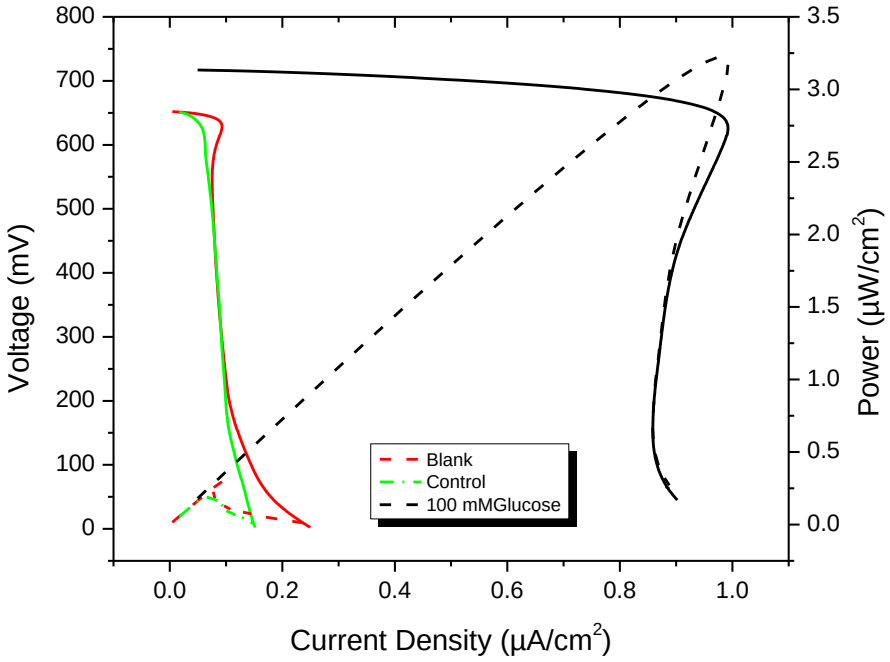

Figure 3.7: Linear polarization curves for the FAD-GDH biofuel cell, voltage (solid), power (dashed). Anode in 150 mM sodium phosphate buffer and 1 mM NQSA, pH 7.2. Cathode in 200 mM citrate/phosphate buffer at pH 4.0

3.4 References

(1) Anastas, P. T.; Chemistry, A. C. S. D. of E.; Meeting, A. C. S. *Green chemistry: designing chemistry for the environment*; American Chemical Society, 1996.

(2) Anastas, P. T.; Bartlett, L. B.; Kirchhoff, M. M.; Williamson, T. C. *Catal. Today* **2000**, *55* (1), 11–22.

(3) Anastas, P. T.; Kirchhoff, M. M.; Williamson, T. C. *Appl. Catal. Gen.* **2001**, *221* (1), 3–13.

(4) Centi, G.; Perathoner, S. *Catal. Today* **2003**, *77* (4), 287–297.

(5) Mateo, C.; Palomo, J. M.; Fernandez-Lorente, G.; Guisan, J. M.; Fernandez-Lafuente, R. *Enzyme Microb. Technol.* **2007**, *40* (6), 1451–1463.

(6) Lykourinou, V.; Chen, Y.; Wang, X.-S.; Meng, L.; Hoang, T.; Ming, L.-J.; Musselman, R. L.; Ma, S. *J. Am. Chem. Soc.* **2011**, *133* (27), 10382–10385.

(7) Letant, S. E.; Hart, B. R.; Kane, S. R.; Hadi, M. Z.; Shields, S. J.; Reynolds, J. G. *Adv. Mater.* **2004**, *16* (8), 689–693.

(8) Liu, B.; Hu, R. *Anal. Chem.* **1997**, *69* (13), 2343–2348.

(9) Liu, W.-L.; Wu, C.-Y.; Chen, C.-Y.; Singco, B.; Lin, C.-H.; Huang, H.-Y. *Chem. - Eur. J.* **2014**, n/a – n/a.

(10) Lee, C.-H.; Lin, T.-S.; Mou, C.-Y. *Nano Today* **2009**, *4* (2), 165–179.

(11) Farrusseng, D.; Aguado, S.; Pinel, C. *Angew. Chem. Int. Ed.* **2009**, *48* (41), 7502–7513.

(12) Potter, M. C. *Proc. R. Soc. Lond. Ser. B Contain. Pap. Biol. Character* **1911**, 260–276.

(13) Sheldon, R. A. *Adv. Synth. Catal.* **2007**, *349* (8-9), 1289–1307.

(14) Sugimoto, Y.; Kitazumi, Y.; Tsujimura, S.; Shirai, O.; Yamamoto, M.; Kano, K. *Biosens. Bioelectron.* **2015**, *63*, 138–144.

(15) Atanassov, P.; Apblett, C.; Banta, S.; Brozik, S.; Barton, S. C.; Cooney, M.; Liaw, B. Y.; Mukerjee, S.; Minteer, S. D. *Interface-Electrochem. Soc.* **2007**, *16* (2), 28–31.

(16) Milton, R. D.; Lim, K.; Hickey, D. P.; Minteer, S. D. *Bioelectrochemistry* **2015**.

(17) Meredith, M. T.; Minson, M.; Hickey, D.; Artyushkova, K.; Glatzhofer, D. T.; Minteer, S. D. *ACS Catal.* **2011**, *1* (12), 1683–1690.

(18) Meredith, S.; Xu, S.; Meredith, M. T.; Minteer, S. D. *J. Vis. Exp. JoVE* **2012**, No. 65.

(19) Moore, C. M.; Akers, N. L.; Hill, A. D.; Johnson, Z. C.; Minteer, S. D. *Biomacromolecules* **2004**, *5* (4), 1241–1247.

(20) Meredith, M. T.; Kao, D.-Y.; Hickey, D.; Schmidtke, D. W.; Glatzhofer, D. T. *J. Electrochem. Soc.* **2011**, *158* (2), B166.

(21) Aquino Neto, S.; Hickey, D. P.; Milton, R. D.; De Andrade, A. R.; Minteer, S. D. *Biosens. Bioelectron.* **2015**, *72*, 247–254.

CHAPTER 4

FUTURE WORK

4.1 Introduction

The ultimate goal of this research has been to forward the progress in making biofuel cells a commercial reality. One of the key limitations holding biofuel cells in the laboratory at a small scale is the instability of enzymes. While there have been noted improvements, including a report of glucose based sensors exhibiting some stability for up to one year[1], the dramatic loss in power over this time frame shows the necessity for immobilization techniques which further enhance stability as well as maintain catalytic activity over time. While this work has shown that enzymatic activity can be achieved and stabilized over several days, exhibiting activity in solution with only minor losses, challenges remain in achieving sufficient enzymatic loading within MOF structures for biofuel cell applications.

There are several avenues of research which deserve further exploration for enzymatic incorporation into MOF structures for biofuel cell production, as well as other commercial uses more generally for creating stable enzyme catalysts. First is finding the maximum loading possible within ZIF-90 while still maintaining the benefits of immobilization. Second is the successful synthesis of MMCF-2 as well as other MOF structures which either incorporate a polyporphyrin, or simply exhibit large planar heme-like ligands, as is the case in MMCF-2 for π stacking of enzymes. Finally is the search for

additional MOFs which are able to be synthesized in mild aqueous conditions as is the case for ZIF-90. Aqueous synthesis affords the combination of synthesis and immobilization into a single process. By discovering additional MOF structures which can be synthesized under aqueous conditions, enzymatic loading can be fine-tuned with the various MOF morphologies.

4.2 ZIF-90 Optimization

Due to the low loading which was achieved using ZIF-90 in the experiments previously conducted, the maximum possible loading needs to be determined. The precise amount of enzyme which can be sustained inside of the MOF structure while still forming will depend on both the size and geometry of the enzymes being immobilized, as well as the inherent porosity of the MOF if another MOF is selected other than ZIF-90. If the enzyme concentration is too high, ZIF-90 will be unable to join nucleation sites and form the distorted crystal structure necessary immobilization. Thus it will be necessary to complete XRD scans of the MOFs prior to completing enzyme concentration assays to confirm that enzymes are in fact immobilized within ZIF-90. After the maximum enzymatic loading has been established, electrochemical experiments will again be repeated in order to determine if sufficiently high enzyme concentrations can be immobilized for an effective biocathode. Even if the maximum loading proves to be insufficient for electrochemistry, the optimization will more generally be useful towards research in reusable enzymatic catalysts throughout a variety of industries, including the chemical and pharmaceutical industries.

4.3 Heme-like MOFs

For much of the last two decades, the majority interest in MOF structures has focused on gas storage[2] or separation[3]. However, as an ever-growing number of stable MOF structures with larger and larger ligands, more focus has shifted to technologies utilizing this extended pore volume afforded by the large ligands. The example discussed in detail previously was MMCF-2[4], which exhibits a heme-like ligand in terms of the π orbitals present for π stacking. In addition to the macrocyclic ligands which have been developed, there is a large body of research using modified porphyrins directly in the ligands, which have found a variety of applications.[5–8]

This new class of heme-like MOF structures has two significant advantages. The first is that since the porphyrin is known to exhibit π stacking, it can be assumed that any enzyme with a heme structure is at the very least a good candidate to self-immobilize. Secondly, due to the large nature of the porphyrin based ligands, the pore volume can be significantly increased, as has been shown for the central pore in MOF-545[9], wherein the central pore of approximately 8 nm is surrounded by 6 smaller cages with pores of 3.6 nm. MOFs which exhibit such large pore dimensions, particularly with heme-like ligands, prove to be exciting candidates for π stacking of heme-containing enzymes.

4.4 Aqueous MOF Synthesis

The majority of MOF structures have been created using solvothermal synthesis techniques, which are unsuitable to incorporate enzymes at the time of MOF synthesis due to both the organic solvents and temperatures required would denature the enzymes. The advantage of the ZIF-90 framework is the ability to synthesize the MOF under aqueous conditions near room temperature such that enzymes will not denature if present

during MOF synthesis. The size-selective sheltering of MOFs synthesized under aqueous conditions removes the size constraints of the pore size to enzyme size since the crystal structure can form around the enzyme and distort the crystal structure to complete encapsulation.

The MOF structures for aqueous synthesis which would be of greatest interest to synthesize under aqueous conditions would be those structures which are electrically conductive. A conductive MOF would facilitate electron transfer between the enzymes and the electrodes and thereby eliminate the need for soluble mediators. Conductive MOFs have gained traction in research in recent years, though aqueous synthesis of conductive MOFs has not yet been thoroughly investigated.[10–12]

4.5 References

(1) Reuillard, B.; Abreu, C.; Lalaoui, N.; Le Goff, A.; Holzinger, M.; Ondel, O.; Buret, F.; Cosnier, S. *Bioelectrochemistry Amst. Neth.* **2015**.

(2) Mason, J. A.; Veenstra, M.; Long, J. R. *Chem. Sci.* **2013**, *5* (1), 32–51.

(3) Rodenas, T.; Luz, I.; Prieto, G.; Seoane, B.; Miro, H.; Corma, A.; Kapteijn, F.; Llabrés i Xamena, F. X.; Gascon, J. *Nat. Mater.* **2015**, *14* (1), 48–55.

(4) Gao, W.-Y.; Niu, Y.; Chen, Y.; Wojtas, L.; Cai, J.; Chen, Y.-S.; Ma, S. *CrystEngComm* **2012**, *14* (19), 6115.

(5) Anderson, J. S.; Gallagher, A. T.; Mason, J. A.; Harris, T. D. *J. Am. Chem. Soc.* **2014**, *136* (47), 16489–16492.

(6) Fateeva, A.; Chater, P. A.; Ireland, C. P.; Tahir, A. A.; Khimyak, Y. Z.; Wiper, P. V.; Darwent, J. R.; Rosseinsky, M. J. *Angew. Chem. Int. Ed.* **2012**, *51* (30), 7440–7444.

(7) Larsen, R. W.; Vetromile, C. M.; Wojtas, L.; Perman, J.; Zaworotko, M. *Biophys. J.* **2011**, *100* (3), 473a – 474a.

(8) Feng, D.; Chung, W.-C.; Wei, Z.; Gu, Z.-Y.; Jiang, H.-L.; Chen, Y.-P.; Darensbourg, D. J.; Zhou, H.-C. *J. Am. Chem. Soc.* **2013**, *135* (45), 17105–17110.

(9) Morris, W.; Volosskiy, B.; Demir, S.; Gándara, F.; McGrier, P. L.; Furukawa, H.; Cascio, D.; Stoddart, J. F.; Yaghi, O. M. *Inorg. Chem.* **2012**, *51* (12), 6443–6445.

(10) Narayan, T. C.; Miyakai, T.; Seki, S.; Dincă, M. *J. Am. Chem. Soc.* **2012**, *134* (31), 12932–12935.

(11) Hendon, C. H.; Tiana, D.; Walsh, A. *Phys. Chem. Chem. Phys.* **2012**, *14* (38), 13120–13132.

(12) Huang, W.; Brosmer, J. L.; Diaconescu, P. L. *New J. Chem.* **2015**.